Atmos. Chem. Phys. Discuss., 14, 9109–9154, 2014
www.atmos-chem-phys-discuss.net/14/9109/2014/
doi:10.5194/acpd-14-9109-2014

Atmospheric Chemistry and Physics Discussions

Insights into characteristics, sources and evolution of submicron aerosols during harvest seasons in Yangtze River Delta (YRD) region, China

Y. J. Zhang[1,2], L. L. Tang[2,1], Z. Wang[1], H. X. Yu[3], Y. L. Sun[4], D. Liu[5], W. Qin[2], H. L. Zhang[6], and H. C. Zhou[1]

[1]Jiangsu Key Laboratory of Atmospheric Environment Monitoring and Pollution Control, School of Environmental Science and Engineering, Nanjing University of Information Science and Technology, Nanjing 210044, China
[2]Jiangsu Environmental Monitoring Center, Nanjing 210036, China
[3]State key laboratory of Pollution Control and Resource Reuse, School of the Environment, Nanjing University, Nanjing 210093, China
[4]State Key Laboratory of Atmospheric Boundary Layer Physics and Atmospheric Chemistry, Institute of Atmospheric Physics, Chinese Academy of Sciences, Beijing 100029, China
[5]Centre for Atmospheric Science, School of Earth, Atmospheric and Environmental Sciences, University of Manchester, Manchester M13 9PL, UK
[6]Handix LLC, Boulder, CO 8031, USA

Received: 19 January 2014 – Accepted: 21 March 2014 – Published: 4 April 2014

Correspondence to: L. L. Tang (lily3258@163.com)

Published by Copernicus Publications on behalf of the European Geosciences Union.

ACPD
14, 9109–9154, 2014

Abstract

Atmospheric submicron particulate matter (PM_1) is one of the most significant pollution components in China. Despite its current popularity in the studies of aerosol chemistry, the characteristics, sources and evolution of atmospheric PM_1 species in the East China are still poorly understood. Particular situations are the two harvest seasons, namely summer wheat harvest and autumn rice harvest. An Aerodyne Aerosol Chemical Speciation Monitor (ACSM) was deployed for online continuous monitoring of PM_1 components during summer and autumn harvest seasons in urban Nanjing situated in the Yangtze River Delta (YRD) region of China. Results show that organic aerosol (OA) was the most abundant PM_1 component, accounting for 39 % and 41 % of the total mass during the summer and autumn harvest periods, respectively. Positive matrix factorization (PMF) analysis resolved three OA components, i.e., hydrocarbon-like OA (HOA), biomass burning OA (BBOA), and oxygenated OA (OOA), which on average accounted for 19 % (30 %), 17 % (18 %), and 64 % (52 %) of the total OA mass concentrations during the summer (autumn) harvest respectively. The BBOA mass fraction increases with an increase of high PM_1 mass loadings ($PM_1 > 100\,\mu g\,m^{-3}$), implying that BBOA plays a dominate role in high PM pollution during the harvest seasons. The mass concentrations of BBOA correlate well with the mass concentration of water-soluble potassium (K^+), indicating that the atmospheric K^+ is a good tracer for both wheat and rice straw burning during the harvest seasons. The BBOA mass concentrations for the summer and autumn harvest can be estimated as BBOA = 36.7 × (m/z 60–0.26 % × OA) and = 41.4 × (m/z 60–0.26 % × OA), respectively, m/z 60 as an identified marker for levoglucosan-like species. The OA mass decreases with the aging of BB plumes, implying that the fresh BB plumes contribute to atmospheric OA burden significantly. Combination of back-trajectory analysis with local wind indicates that the heavy pollution during the harvest seasons in the YRD region was found to be associated with transport processes and local source emissions.

ACPD
14, 9109–9154, 2014

1 Introduction

Particulate matter (PM) that is suspended in the atmosphere as atmospheric aerosol plays a crucial role in regional and global climate system (Ramanathan et al., 2001; Kaufman et al., 2002), air pollution (Sun et al., 2013a), ambient visibility reduction (Watson, 2002) and human health (Ge et al., 2011). Significant amounts of PM can be generated from human activities. In particular, biomass burning (BB) activities, e.g., forest fires, wildfire, and agricultural fires, can become the main sources of fine particulate matter ($PM_{2.5}$, particulates $\leq 2.5\,\mu m$ in aerodynamic diameter) and/or submicron particulate matter (PM_1, particulates $\leq 1\,\mu m$ in aerodynamic diameter) (Andreae and Merlet, 2001, Aiken et al., 2010; DeCarlo et al., 2010; Lee et al., 2010; Cubison et al., 2011; Reche et al., 2012; Bougiatioti et al., 2013). In recent years, the broad spatial extent of the atmospheric pollution frequently occurs during harvest seasons in China because of agricultural fires (Li et al., 2007; Wang et al., 2009a; Li et al., 2010; Du et al., 2011; Cheng et al., 2013; Ding et al., 2013). Moreover, China is an agricultural country which has 1.8 billion cultivated fields with a large number of agricultural crop residue (Zhang et al., 2008). The understanding of the compositions, sources and processes of atmospheric aerosol particles during harvest seasons is urgently needed to design measures to improve the quality of air in China.

Organic aerosol (OA) composes a large fraction of atmospheric aerosol particles (Zhang et al., 2007). Thus, one main research focus is the source identification of atmospheric OA (e.g. Lanz et al., 2007, 2010; DeCarlo et al., 2010; He et al., 2010; Crippa et al., 2013b; Hu et al., 2013; Sun et al., 2013a). The emission sources of atmospheric OA are usually identified by positive matrix factorization (PMF) method (Paatero and Tapper, 1994; Paatero, 1997). The current PMF method can only be employed to analyze the OA datasets (Sun et al., 2012b; Zhang et al., 2011), but cannot be easily utilized in the real-time online understanding of atmospheric OA sources. To identify the sources of atmospheric OA online, an algorithm based solely on organic mass fragments, namely m/z 57 (mostly $C_4H_9^+$) and m/z 44 (mostly CO_2^+), were devel-

ACPD
14, 9109–9154, 2014

oped to estimate hydrocarbon-like OA (HOA) and oxygenated OA (OOA), respectively (Zhang et al., 2005a, b; Ng et al., 2011c). Mohr et al. (2012) also identified cooking OA (COA) in ambient datasets based on the fractions of COA tracers at m/z 55 (mostly $C_4H_7^+$) and m/z 57 organic mass fragments. Biomass burning organic aerosol (BBOA) is one of the major atmospheric OA species during biomass burning periods (Aiken et al., 2010; Allan et al., 2010). However, limited information is available for developing online technique for the source appointments of BBOA.

The evolution of atmospheric OA such as oxidation process can significantly influence the ambient concentrations and physicochemical properties of OA (Aiken et al., 2008; Jimenez et al., 2009; Sun et al., 2011). To date various methods have been developed and introduced to predict the oxidation process of atmospheric OA. Atomic oxygen-to-carbon (O: C) ratios measured by a high-resolution time-of-flight aerosol mass spectrometer (HR-ToF-AMS) have been employed to determine the oxidation state of ambient OA (Aiken et al., 2008). Carbon oxidation state has been also used to evaluate the degree of OA oxygenation (Kroll et al., 2011). A tracer-CO (OA/ΔCO) has been found to be an effective method for understanding the photochemical oxidation process of OA in the atmosphere (Jolleys et al., 2012; Hu et al., 2013). In addition, Ng et al. (2010 and 2011b) addressed that a triangular region, f_{44} (fraction of m/z 44 in total OA) vs. f_{43} (fraction of m/z 43 in total OA), can be used to evaluate the oxidation processing of OA. Cubison et al. (2011) also found that f_{44} as a function of f_{60} (fraction of m/z 60 in total OA) can be utilized to understand the aging of BBOA and estimate the background value of f_{60}, indicating the formation and transformation of primary and secondary BBOA from the BB plumes. It is important for understanding the nature of atmospheric OA to investigate the evolution of OA by means of a proper technique.

An Aerodyne Aerosol Chemical Speciation Monitor (ACSM), a new instrument is designed as the state-of-the art research grade Aerodyne Aerosol Mass Spectrometer (AMS) systems to routinely characterize and monitor the mass and chemical composition of non-refractory submicron particulate matter (NR-PM_1), i.e., OA, nitrate (NO_3), sulfate (SO_4), ammonium (NH_4), and chloride (Chl) in real time (Canagaratna et al.,

ACPD
14, 9109–9154, 2014

2007; Ng et al., 2011a; Sun et al., 2012a). Furthermore, ACSM has been found to have lower size, weight, cost, and power requirements in comparison with AMS (Ng et al., 2011a; Sun et al., 2012a). In recent years, air pollution and haze weather have become more and more important environmental and meteorological issues in Yangtze River Delta (YRD) region of China (Du et al., 2011; Ding et al., 2013). It was the purpose of this study to investigate the characteristics, sources and evolution of PM_1 using ACSM during harvest seasons (summer wheat harvest and autumn rice harvest) in the YRD region, China. The diurnal variations of the mass concentrations of non-refractory species (OA, NO_3, SO_4, NH_4, Chl) and black carbon (BC) in the PM_1 were characterized during the harvest seasons. The emission sources of organic compositions (HOA, BBOA, and OOA) in the NR-PM_1 were traced by means of the PMF model. Based on m/z 60 mass concentration, the mass concentrations of BBOA in the NR-PM_1 were reconstructed online. Furthermore, the evolution process of OA during the harvest seasons was investigated by online measurements. Combination of back-trajectory analysis of air masses with local wind was used to investigate the impacts of various source regions on the PM pollution during the harvest seasons.

2 Experimental methods

2.1 Sampling site description

With a population of more than 8 million and an area of about 6597 km^2, Nanjing, the host city of the second Youth Olympic Games in 2014, is a representative Chinese city in terms of the pollution characteristics of the YRD region. In this study, all kinds of data was collected in urban Nanjing (118°46′ N, 32°05′ E) from 1 to 15 June, and 15 to 30 October 2013, corresponding to two harvest seasons in a year, namely summer wheat harvest and autumn rice harvest. The sampling site was located on the roof of a six-story building approximately 18 m a.g.l. and 25 m from heavy-traffic road and restaurants in this study.

ACPD
14, 9109–9154, 2014

2.2 Instrumentation and data analysis

2.2.1 Measurements

The ambient NR-PM_1 species, i.e., OA, NO_3, SO_4, NH_4, Chl, were continuously measured using ACSM from 1 to 15 June, and 15 to 30 October 2013. Detailed descriptions of ACSM can be found in previous studies (Ng et al., 2011a; Sun et al., 2012a). Briefly, the ambient aerosols were drawn into the room using a 1/2 inch (outer diameter) stainless steel tube at a flow rate of $\sim 3\,\mathrm{L\,min^{-1}}$, of which ~ 84 cc $\mathrm{min^{-1}}$ was sub-sampled into the ACSM. Moreover, ACSM was operated at a time resolution of about 15 min with a scan from m/z 10 to 150 amu at 500 ms amu^{-1} rate, which corresponds to the settings of Sun et al. (2012a).

An online analyzer, Monitoring of Aerosols and Gases (MARGA, model ADI 2080 Applikon Analytical B. V. Corp., the Netherlands), was deployed to measure the mass concentrations of a major water-soluble inorganic ion (potassium ion, K^+) in the aerosols. A $PM_{2.5}$ cyclone inlet was used to remove coarse particles. Ambient air was sampled into a liquid with a flow rate of $16.7\,\mathrm{L\,min^{-1}}$. The detection limits of K^+ is $0.09\,\mu\mathrm{g\,m^{-3}}$.

The MET ONE BAM-1020 and the 7-wavelength aethalometer (Magee AE31) were employed to measure PM_1 and ambient atmospheric BC in $PM_{2.5}$, respectively. Various gas analyzers (Thermo Scientific), i.e., Model 49i, Model 48i, and Model 42i, were collocated for monitoring O_3, CO, and NO_2, respectively. Ambient meteorological parameters including ambient temperature (T), relative humidity (RH), precipitation, wind speed (WS), wind direction (WD), and atmospheric visibility were obtained from a ground meteorology station located on the same six-story building as the sampling site.

Fire products used in this study were available from MODIS (Moderate-resolution Imaging Spectroradiometer) mounted on NASA's Terra and Aqua satellites, NASA's Earth Observing System (EOS) (https://earthdata.nasa.gov/data/near-real-time-data/firms). MODIS can present fire distributions in details at 1 km resolution through Fire

ACPD
14, 9109–9154, 2014

Information for Resource Management System (FIRMS) on global scale (Justice et al., 2002; Kaufman et al., 2003). As shown in Figs. S1 and S2, all agricultural fire locations (red dots) in the YRD region were detected by the remote sensing retrieval of MODIS from 1 to 15 June, and 15 to 30 October 2013 (http://firms.modaps.eosdis.nasa.gov/firemap/).

2.2.2 ACSM data analysis

An ACSM Data Analysis Software package, ACSM Local (Ver. 1.5.2.0.0, released 25 April 2012) written in Wavemetrics Igor™, was used to analyze the ACSM dataset. More details of procedures have been described in the studies of Ng et al. (2011a) and Sun et al. (2012a). The relative ionization efficiencies (RIEs) values usually used in AMS ambient concentration calculations (Canagaratna et al., 2007) are the default values of NO_3 (1.1), SO_4 (1.2), and Chl (1.3) in this study. Moreover, a RIE value of NH_4 was determined to 7.04 based on the measurement of pure ammonium nitrate (NH_4NO_3) particles. In addition, the mass concentrations of ambient aerosol need to be corrected for particle collection efficiency (CE) (Middlebrook et al., 2011). CE = 0.5 is found to be representative with data uncertainties generally within 20 % (Canagaratna et al., 2007; Middlebrook et al., 2011). The CE values observed in previous studies range from 0.43 to 1, due to (a) shape-related collection losses at the vaporizer from inefficient focusing of non-spherical particles, (b) particle losses at the vaporizer because of bouncing of solid particles before they are completely vaporized, and (c) particle losses in the aerodynamic inlet as a function of particle diameter (Allan et al., 2004; Zhang et al., 2005b; Canagaratna et al., 2007; Middlebrook et al., 2011). In this study, we selected the CE value for OA, NO_3, SO_4, NH_4, and Chl, respectively, according to the equation CE = max (0.45, 0.0833 + 0.9167 × ANMF) (Middlebrook et al., 2011), in which ANMF is the mass fraction of NH_4NO_3 measured by the ACSM.

The PMF method was also applied to analyze OA datasets from ACSM. More details of procedure for PMF model can be found in previous studies (Ulbrich et al., 2009; Zhang et al., 2011; Sun et al., 2012b). Furthermore, the OA mass spectra data from

ACPD
14, 9109–9154, 2014

ACSM were determined by combing PMF2 executables with the PMF Evaluation Tool (PET) (Ulbrich et al., 2009). Due to large interferences of internal standard of naphthalene at m/z's 127–129, the PMF analysis was restricted to m/z 120 (Sun et al., 2012a, 2013a). Three factors (HOA, BBOA, and OOA) were identified in this study.

2.2.3 Back-trajectory analysis

The impacts of various source regions on the PM pollution during the harvest seasons have been investigated using the HYbrid Single Particle Lagrangian Integrated Trajectory (HYSPLIT-4) model developed by NOAA/ARL (Draxler and Rolph, 2003). Accordingly, 48 h back-trajectories at 500 m arrival height a.g.l. were calculated every 2 h starting at China Standard Time (CST) based on a Trajectory Statistics (TrajStat) software developed by Wang et al. (2009b). In this study, the 48 h back-trajectories of air masses were used for further analysis.

3 Results and discussion

3.1 Meteorological factors and PM_1 components

3.1.1 Time series of meteorological factors and PM_1 components

Figure 1 depicts the time series of NR-PM_1 species and BC in the presence of different meteorological conditions during the harvest seasons in urban Nanjing, i.e., WS, WD, RH, T, and precipitation. During the summer harvest, the average values were 70.7 ± 15.3 %, $3.7 \pm 1.7\,m\,s^{-1}$, and 23.4 ± 4.1 °C for the ambient RH, WS, and T, respectively. In the autumn harvest, the average values were 54.3 ± 13.7 %, $2.6 \pm 1.4\,m\,s^{-1}$, and 18.1 ± 3.6 °C for the ambient RH, WS, and T, respectively. The frequency distribution of hourly averaged wind direction and speed throughout the summer and autumn harvests were shown in Fig. S2a and b. As shown in Fig. S3, there is a strong correlation between the MET ONE PM_1 measured by MET ONE BAM-1020 and the sum of

ACPD
14, 9109–9154, 2014

NR-PM_1 and BC mass concentrations (r^2 = 0.88), indicating that the ambient submicron aerosols consisted mainly of the NR-PM_1 and BC. Note that the mass concentration of BC in the PM_1 may be overestimated due to the fact that the mass concentration of BC was measured by the 7-wavelength aethalometer for $PM_{2.5}$ and the uncertainties in converting measured light absorption coefficients to carbon concentrations. An overestimation was previously suggested by Huang et al. (2011).

During the summer harvest, PM_1 (NR-PM_1 + BC) consisted of OA (39 %), NO_3 (23 %), NH_4 (16 %), SO_4 (12 %), BC (8 %), and Chl (1 %). During the autumn harvest, PM_1 was composed of OA (41 %), NO_3 (20 %), NH_4 (14 %), SO_4 (11 %), BC (13 %), and Chl (1 %). In particular, OA exhibited a significant dynamic variation in mass concentrations during the harvest seasons, likely due to the changes of source emissions (i.e. cooking, traffic and/or BB emissions). For example, the OA mass concentration sharply increased into 145.4 $\mu g\,m^{-3}$ at 21:00 local time (LT) on 10 June, while the PM_1 mass concentration reached 253.0 $\mu g\,m^{-3}$. Table 1 presents a comparison of the average composition of PM_1 between the summer harvest and autumn harvest periods. In contrast to SO_4 and NH_4, all other submicron species were higher during the autumn harvest than during the summer harvest. In addition, it was found that the highest peak values of PM_1 during the harvest seasons primarily depend on primary OA (POA), such as HOA, and/or BBOA at the sampling site (see Sect. 3.3).

3.1.2 Diurnal variations of meteorological factors and PM_1 components

Figure 2 depicts the diurnal variations of the meteorological factors, i.e., RH, T, WS, and WD, and PM_1 species, i.e., OA (including HOA, BBOA, and OOA), NO_3, SO_4, NH_4, Chl, and BC. Generally, the diurnal variations of the meteorological parameters and PM_1 species are similar during the summer harvest and autumn harvest. However, the ambient RH and T during summer harvest were higher than those during autumn harvest.

ACPD
14, 9109–9154, 2014

OA obviously exhibit three peaks occurring between 6:00–8:00 LT, 11:00–14:00 LT, and 19:00–22:00 LT, which is in agreement with the emission behaviors of pollution sources i.e., traffic, cooking and/or BB emissions (Allan et al., 2010; Huang et al., 2012; Sun et al., 2012a; Crippa et al., 2013a). More details of the diurnal variations of the OA components, i.e., HOA, BBOA, and OOA, will be presented in Sect. 3.2.

The diurnal variation of SO_4 presents three peaks during the summer and autumn harvest. A minor peak of SO_4 appeared in the morning at around 08:00 LT possibly influenced by sulfur-containing fuel. The second slight peak in the early afternoon at 13:00 LT formed by tracer gas (SO_2) oxidation under a higher photochemical activity, which is consistent with high temperature. Note that a third peak at night (22:00 LT) was observed which is interpreted to be due to a formation of SO_4 via an aqueous-phase oxidation reaction (Sun et al., 2013b). Overall, the SO_4 mass shows a relatively flat trend, indicating a regional pollution of sulfur components during harvest seasons in the YRD region.

NO_3 and Chl show similar diurnal cycles with two distinct peaks in the morning (07:00–08:00 LT) and in the evening (20:00–23:00 LT) for chloride, and a lower concentrations in the afternoon 11:00–17:00 LT during the harvests, in accordance with the volatile properties of ammonium nitrate and ammonium chloride dependent on ambient T and RH (Sun et al., 2011, 2012a). Chl is mainly ammonium chloride (NH_4Cl) and/or organic chlorine-containing species. During the harvest seasons, the evening high values of NO_3 and Chl might be affected by BB emissions and/or formed via gas-phase and aqueous-phase oxidations.

In addition, NO_3 shows a minor peak in the early afternoon (12:00–13:00 LT) during the autumn harvest, due to the gas-phase photochemical production of nitric acid (HNO_3) overcoming the evaporative loss at higher high T (Sun et al., 2011). However, the decrease of NO_3 during the summer harvest is quicker than the one during the autumn harvest. This is because that the photochemical production of HNO_3 cannot compensate for the evaporative loss at a high T condition during the summer harvest. BC shows a classic diurnal variation with higher loadings appearing in early morn-

ACPD
14, 9109–9154, 2014

ing and during nighttime, which is consistent with traffic rush hours in early morning (07:00–08:00 LT) and during nighttime (20:00–21:00 LT). In addition, the reason for the peak values of BC during the nighttime may be also caused by the BB emissions during these harvest seasons.

3.2 Organic source apportionment

Based on the OA dataset from ACSM, the PMF analysis was performed for 1 to 8 factors. Three components (i.e. HOA, BBOA, and OOA) were identified, as illustrated in Figs. 3 and 4. The mean mass concentrations of HOA, BBOA, and OOA during the harvest seasons were presented in Table 1. HOA, BBOA, and OOA accounted on average for 19 % (30 %), 17 % (18 %), and 64 % (52 %) of the total OA mass concentrations during the summer (autumn) harvest, respectively. In particular, the average contribution of BBOA for the summer harvest is similar to that for the autumn harvest.

3.2.1 Hydrocarbon-like OA (HOA)

The prominent hydrocarbon ion series of $C_nH^+_{2n+1}$ and $C_nH^+_{2n-1}$ (e.g. 27, 29, 41, 43, 55, 57,...) obtained from mass spectrum were characterized as the components of HOA (Zhang et al., 2005a, 2011; Aiken et al., 2008; Mohr et al., 2009; Allan et al., 2010). m/z 57 ($C_3H_5O^+$ and/or $C_4H_9^+$) and m/z 55 ($C_3H_3O^+$ and/or $C_4H_7^+$) are commonly considered as tracers for the primary organic emissions of combustion sources in urban areas, including COA and HOA (Zhang et al., 2005a; Ng et al., 2010; Sun et al., 2012a, 2013a; Hu et al., 2013). It is found that there is no significant difference in the mass spectrum between the summer harvest and the autumn harvest (Fig. 3a). Compared with traffic-like OA (Liu et al., 2011; Crippa et al., 2013a), the mass spectrum obtained in the present study shows a higher m/z 55/57 ratio. Previous studies indicated that high m/z 55/57 together with a unique diurnal variation can be as a diagnostics for the presence of COA (Mohr et al., 2009; Allan et al., 2010; Sun et al., 2012a). The mass spectrum of HOA in this study is characterized by more abundant

ACPD
14, 9109–9154, 2014

ions, i.e., m/z 41 (mainly $C_3H_5^+$), m/z 55 (mainly $C_4H_7^+$) and m/z 57 (Fig. 3a), which is similar to the characteristics of COA mass spectrum measured by He et al. (2010). As shown in Fig. 2, the diurnal variation of HOA shows three pronounced peaks corresponding to morning (a slight peak), noon (a weak peak) and evening traffic/cooking activities (a strong peak). In the meanwhile, the HOA mass loadings show weak correlations with the mass concentrations of CO (r^2 = 0.11 and 0.35, Fig. 4e), indicating that COA may significantly contribute to the HOA species. Differences in r^2 values between the two harvest seasons could be caused by different pollution types (Zhang et al., 2005a). Hence, HOA in this study refers to the sum of traffic-related HOA and COA. Sun et al. (2010) and Sun et al. (2012a) also found that HOA species in urban ambient were influenced by both traffic and cooking-like activities.

3.2.2 Biomass burning OA (BBOA)

As shown in Fig. 3b, the mass spectrum of BBOA extracted in this study shows a prominent peak of m/z 60 which is a well-known tracer ion for biomass burning emissions (Alfarra et al., 2007; Aiken et al., 2009; Cubison et al., 2011; Huang et al., 2011; Liu et al., 2011). Levoglucosan was shown to contribute to m/z 60 and was found in large amounts in urban, suburban, and rural background atmosphere during biomass burning periods (Maenhaut et al., 2012). Using soluble K^+ as a tracer for BB has also been reported by previous analyses of biomass burning campaign data (Gilardoni et al., 2009; Aiken et al., 2010; Li et al., 2010; Du et al., 2011; Crippa et al., 2013a). Figure 4a shows the time series of BBOA mass concentration along with K^+ measured by MARGA. The BBOA mass concentration is strongly consistent with the K^+ mass concentration (r^2 = 0.96) during summer harvest (Fig. 4d), suggesting that BBOA and K^+ were as expected from the same source. K^+ can thus be used as a tracer for biomass burning particles as well. In particular, K^+ can be a species for identifying the wheat straw burning emissions. As shown in Fig. 4d, the BBOA is also well correlated with K^+ in summer (r^2 = 0.64), which further verifies that the BBOA is a significant source in both periods. Sullivan et al. (2008) also found that the concentration of levoglucosan

ACPD
14, 9109–9154, 2014

correlates with K^+ for the burning of rice straw. Therefore, results above suggest that the atmospheric K^+ also can be used as a species for identifying the wheat and rice straw burning emissions during the harvests. In addition, the diurnal variation of BBOA shows a pronounced peak at the nighttime, which is consistent with the effects of the BB activities (Fig. 2). This means that BBOA contributes to POA during the nighttime mainly. The BBOA identified in this study is an expected result due to extensive fire counts around the sampling site during this campaign, as shown in Fig. S1a and b. This finding is also consistent with the habit of the farmers in the YRD region to burn off wheat or rice straw during harvest seasons each year. Furthermore, the mass concentration of Chl correlates well with the BBOA loadings (r^2 = 0.87 and 0.56), but Chl and HOA shows no correlations (r^2 = 0.07 and 0.001) during the harvest seasons (Fig. S4). This confirms that Chl was mainly from the BB emissions.

3.2.3 Oxygenated OA (OOA)

OOA, as a surrogate of secondary organic aerosol (SOA), is one of the most important secondary sources of atmospheric submicron aerosols in China (Xiao et al., 2011; Huang et al., 2012; Sun et al., 2012a). The mass spectrum of both OOA components in Fig. 4c were characterized by the prominent $C_xH_yO_z^+$ fragments, mainly CO_2^+ (m/z 44) which has been denoted previously found in many AMS studies (Zhang et al., 2005a; Jimenez et al., 2009; Sun et al., 2010). As shown in Fig. 4f, the OOA mass concentration correlates well with the sum of NO_3 and SO_4 (r^2 = 0.57 and 0.59) during the summer and autumn harvests, respectively. In addition, the diurnal pattern of OOA is characterized two peaks at around 14:00–15:00 LT, suggesting that OOA might be formed by photo-oxidation of precursors in the afternoon. Note that OOA also exhibits high loadings during the nighttime. This may be caused by the aging of BB plumes (Jolleys et al., 2012). In addition, it was also observed that RH are generally high (~ 70 %) during the nighttime, implying that aqueous-phase oxidations may contribute to the generation of OOA significantly (Heringa et al., 2011; Li et al., 2013). Similar to OOA, BBOA was also enhanced during the nighttime (Fig. 2).

ACPD
14, 9109–9154, 2014

3.3 Effects of chemical components on PM pollution

As shown in Fig. 5a and b, the total PM_1 species and atmospheric visibility show strongly dynamic variations during no/negligible biomass (wheat and/or rice straw) burning (non-BB) and biomass burning (BB) periods in urban Nanjing, respectively. The average mass concentration of total PM_1 was 49 (58.9) $\mu g\,m^{-3}$ during summer (autumn) BB periods, which is around two times more than that during summer (autumn) non-BB periods with the average mass concentration of 23.4 (28.6) $\mu g\,m^{-3}$. The contribution of OA to the total PM_1 species is 34 % (37 %) during the summer (autumn) non-BB periods, but the contribution reaches to 41 % (48 %) during the summer (autumn) BB periods. This means that a further investigation on OA components needs to be considered in PM pollution during the harvest seasons. As a matter of fact, the average mass concentrations of all OA components (i.e. HOA, BBOA, and OOA) increase during the BB periods. In addition, the average atmospheric visibility is 10.6 (8.1) km during summer and autumn non-BB period. However, the atmospheric visibility shows obvious reduction during summer and autumn BB period with the mean value of 11.9 and 6.5 km. These findings indicate that the BB pollution is a possible reason for the haze formation in urban Nanjing, at least to some extent. Wang et al. (2009a) also found that wheat straw burning mainly contributed to atmospheric aerosol during haze days in urban Nanjing.

All the mass concentrations and fractions of the PM_1 components, i.e., SO_4, NO_3, NH_4, Chl, BC, HOA, BBOA, and OOA, are a function of the PM_1 mass concentration during the harvest seasons, respectively (Fig. 6). The secondary species mass concentrations, i.e., SO_4, NO_3, NH_4, and OOA, show monotonic and almost linear increase with the increase of the PM_1 mass concentrations, which is in agreement with results during the pollution periods in Beijing, China (Sun et al., 2013a). In particular, the mass concentrations of BBOA and Chl, present almost exponential increase with the increasing of PM_1 loadings during the whole campaign. In addition, the mass concentrations of BC and HOA show no clear relationships with PM_1 the loadings, but for

ACPD
14, 9109–9154, 2014

$PM_1 < 90\,\mu g\,m^{-3}$ the mass concentrations of BC and HOA display a monotonic and almost linear relationship. The HOA mass concentration (including both traffic and cooking) has stable values at $70\,\mu g\,m^{-3} < PM_1 < 100\,\mu g\,m^{-3}$, and then decreases to relatively lower values. The secondary inorganic species, except NO_3, contributions to PM_1 loadings show almost linear decrease with PM_1 from ~ 25 % to 5 % with the increase of PM_1 loadings. NO_3 shows two minor peaks at $60\,\mu g\,m^{-3} < PM_1 < 70\,\mu g\,m^{-3}$ and $90\,\mu g\,m^{-3} < PM_1 < 100\,\mu g\,m^{-3}$. HOA shows a peak at $70\,\mu g\,m^{-3} < PM_1 < 80\,\mu g\,m^{-3}$. Generally, the BBOA and Chl mass fractions show similar trend to the BBOA and Chl mass concentration as a function of the PM_1 mass loadings, respectively. In particular, BBOA is a main contributor to the increasing of PM_1 loadings as the PM_1 loadings are larger than $100\,\mu g\,m^{-3}$. On the other hand, Chl shows a relatively small contribution to PM_1 across all the mass loadings. BC and OOA show relatively stable contributions to the PM mass loadings. Hence, more prominent peaks values of organics in this study were mainly attributed to POA (including traffic-related HOA, COA, and BBOA) emissions. In addition, the results suggest that BBOA plays a key role in causing the highest PM pollution during the harvest seasons, whereas the role of secondary species is less significant. Additionally, for the PM_1 loadings of 70–80 $\mu g\,m^{-3}$ and 90–100 $\mu g\,m^{-3}$, NO_3 has an important impact on PM during the harvest seasons in the YRD region.

As shown in Fig. 7a, POA dominates the OA mass fraction when the PM_1 loadings are high during the harvest seasons. For example, when the mass fraction of OA is > 70 %, the POA mass concentration reaches ~ $100\,\mu g\,m^{-3}$, while SOA is generally below ~ $10\,\mu g\,m^{-3}$. This is because that BBOA accounted for a larger fraction of OA when the PM_1 loadings were > $100\,\mu g\,m^{-3}$. Though the POA loadings exceed SOA loadings at higher PM_1 loadings during the entire study, the mass concentration of SOA is always on average higher than that of POA throughout the whole day (Fig. 7b). In particular, the mass fraction of OA is > 60 % at 13:00–17:00 LT, which may be due to the high formation of photochemical products during the daytime. In general, the average mass concentrations of POA and SOA during the summer and autumn harvest seasons are 5.1 (9.3) $\mu g\,m^{-3}$ and 9.27 (10.1) $\mu g\,m^{-3}$, accounting for 36 % (64 %) and

ACPD
14, 9109–9154, 2014

48 % (52 %) during the summer (autumn) harvest, respectively. As shown in Table 1, the POA loadings during the autumn harvest are around 2 times higher than that during the summer harvest in urban Nanjing. This was probably caused by the amount of the fire sites around the urban Nanjing in the YRD region (Fig. S1a and b).

The effects of total primary and secondary species on the PM pollution during the harvest seasons were also investigated. Generally, the secondary PM (SPM = $SO_4 + NO_3 + NH_4 + OOA$) is higher than the primary PM (PPM = HOA + BBOA + BC), as shown in Fig. 7c and d. Although the BBOA mass fraction in OA is higher, BBOA/OA was indicated > 45 %, the SPM mass concentration is higher than the PPM mass concentration, suggesting that the secondary aerosol with high loadings were formed during the BB campaigns (Fig. 7c). As shown in Fig. 7d, the diurnal cycles of the PPM and SPM mass fractions show that SPM accounted for larger fraction in PM_1 during the whole day. The contribution of SPM to PM_1 varies from 50 % to 72 %, and the highest contribution occurs at 15:00–16:00 LT. The average contribution of SPM and PPM for the entire study was 59 % and 41 %, respectively. Thus, aforementioned results imply that SPM also plays an important role in the PM pollution during the harvest seasons even if the POA loadings overwhelm the loadings of SOA in OA.

3.4 Estimation of BBOA directly from a tracer (m/z 60)

The BBOA mass loadings during the harvest seasons were estimated using a simple method. As described in previous studies, the parameter f_{60}, fraction of m/z 60 in total OA, is considered as a marker of BBOA (Alfarra et al., 2007; DeCarlo et al., 2008; Cubison et al., 2011). To estimate the real value of the BBOA loadings, the background level of f_{60} (0.26 ± 0.1 %) during non-BB periods was determined (Fig. 8a). Cubison et al. (2011) also obtained a similar background level of f_{60}(0.3 ± 0.06 %) for an urban city in Mexico. Therefore, the levoglucosan-like species in ambient BB plumes was estimated by $\Delta m/z$ 60 ($\Delta m/z$ 60 = m/z 60 – background value of f_{60} × OA). As shown in Fig. 9, the strong correlations (r^2 = 0.98, Slope = 36.7 and r^2 = 0.96, Slope = 41.4) between the BBOA mass concentration and $\Delta m/z$ 60 were observed during the sum-

ACPD
14, 9109–9154, 2014

mer and autumn harvest. Aiken et al. (2009) also found that BBOA mass concentration strongly correlates with $\Delta m/z$ 60 mass loadings ($r^2 = 0.91$, Slope = 34) during the biomass burning/woodsmoke periods in Mexico City. Furthermore, Lee et al. (2010) obtained a strong relationship between BBOA mass concentration and m/z 60 mass loadings ($r^2 = 0.92$, Slope = 34.5) through a wildland fuels fire experiment in the lab. Thus, we reconstructed the time series of BBOA mass concentration to compare the relationship between the extracted BBOA mass concentration by PMF modeling (PMF BBOA) and the estimated BBOA mass concentration. As shown in Fig. 10a and b, excellent agreement is observed between the identified and reconstructed BBOA concentrations during the summer harvest (Slope = 0.94 and $r^2 = 0.98$) and the autumn harvest (Slope = 1.06 and $r^2 = 0.96$). Therefore, the BBOA component during the BB campaigns in urban Nanjing of the YRD region can be estimated with the equations of BBOA = 36.7 × (m/z 60–0.26 % × OA) and BBOA = 41.4 × (m/z 60–0.26 % × OA) for the summer and autumn harvest, respectively.

3.5 Oxidation process of OA

Figure 11 depicts the overall mass concentration and fraction of OOA and the OA/ΔCO ratio as a function of O_x ($O_x = O_3 + NO_2$), respectively, to investigate further the probable importance of photochemical activity for organic oxidation. The CO background is determined as 49 $\mu g\,m^{-3}$ based on an average of the lowest 5 % CO during two plumes (Takegawa et al., 2006). As shown in Fig. 11a, the variation of average mass concentration of OOA shows a relatively stable with the increasing of O_x concentration, which is mainly due to larger OOA loadings during the nighttime (Fig. 2). The average fraction of OOA shows a linear relationship with the O_x concentration, as the O_x concentration increases from $\sim 90\,\mu g\,m^{-3}$ to $> 200\,\mu g\,m^{-3}$ (Fig. 11b). Whereas the OOA mass fraction decreased as the O_x concentration increased between 0 and 90 $\mu g\,m^{-3}$. A lower OOA fraction is associated with a large POA concentration during the nighttime, which also agrees well with the results shown in Fig. 2. In addition, the OA/ΔCO ratios can be used to further analysis the formation and evolution processes of SOA, which has

ACPD
14, 9109–9154, 2014

been employed in many previous studies (de Gouw et al., 2005; Jimenez et al., 2009; DeCarlo et al., 2010; Jolleys et al., 2012; Hu et al., 2013). As shown in Fig. 11c, the OA/ΔCO is a function of O_x, implying that photochemical activity might play an important role in the OOA formation. In particular, OA/ΔCO shows a small peak at 30 µg $m^{-3} < O_x < 80$ µg m^{-3}, which indicates that OOA formation occurs likely via the condensation of the less volatile products of these aging reaction on the particles during nighttime under the conditions of low T and high RH (Jimenez et al., 2009; Ng et al., 2010, 2011b). These findings suggest that gas-phase oxidation during the daytime is likely to be the main driving force for the OA oxidation under stronger photochemical activity condition, while particle-phase and/or condensation processes may have been responsible for the high degree of oxygenation of OA during the nighttime under the high RH.

Figure 12a depicts the evolution process of OA with the f_{44} vs. f_{43} space during the summer and autumn harvests. As increasing the mass loadings of O_x the ambient OA components cluster within a well-defined triangular region of the plot, implying that the degree of OA aging might be affected by atmospheric photochemical activity. Note that the ambient OA initially is on the left side of the triangle, but on the O_x increasing moved slight up and to the right, clusters into the triangle, suggesting that the fresh BB emissions have a rather low relative contribution to f_{43}, but the m/z 43 ladings increase with the increasing of f_{44}. This is consistent with the results of photo-oxidation smog chamber experiments carried out by Heringa et al. (2011). In the study by Heringa et al. (2011), the non-oxidized fragment $C_3H_7^+$ has a considerable contribution at m/z 43 for the fresh OA with an increasing contribution of the oxygenated ion $C_2H_3O^+$ during aging of BB emissions.

The formation and transformation of primary and secondary BBOA during the BB campaigns can be described by f_{44} vs. f_{60} plot (Cubison et al., 2011). As shown in Fig. 8a, the fraction of BBOA decreases with increasing the oxidation degree of OA. During the photochemical activity campaign, the lower is the BBOA/ΔCO ratio the higher is the oxidation degree of OA (Fig. 8b). These findings suggest a potential mech-

ACPD
14, 9109–9154, 2014

anism by which fresh BB plumes undergoes the substantial photochemical oxidation and is transformed into aged BB plumes. Therefore, atmospheric photochemical activity might play an important role in the aging process of open BB plumes during the summer and autumn harvests. In addition, Fig. 12b depicts the evolution process of the BB plume with f_{44} vs. f_{60} spaces during the harvest seasons. As decreasing the mass of the total PM_1 the OA components cluster within a higher oxidation region of the plot, i.e., higher f_{44} and lower f_{60} region, suggesting that the contribution of the fresh BB plume to the PM pollution gradually decreases with the aging of evolving ambient open BB plumes. Furthermore, the OA loadings also decrease gradually with the aging of open BB plumes. Thus, it is reasonable to believe that the fresh BB plumes significantly contribute to the ambient OA burden during the harvest seasons.

3.6 Impacts of various source regions on the PM pollution

Figure 13 presents the calculated air mass 48 h BTs at 500 m arrival height a.g.l. at intervals of two hours (i.e. 00:00, 02:00, 04:00, ..., 22:00 LT) starting at CST in Nanjing (118°46′ N, 32°05′ E). The corresponding BTs can be broadly classified into four groups based on the directions during the summer and autumn harvests, respectively, i.e., southwest (Group 1), east (Group 2), northwest (Group 3), and northeast (Group 4) for the summer harvest; northwest (Group 1), east (Group 2), south (Group 3), and northeast (Group 4) for the autumn harvest season. The mean concentrations of PM_1 in this study are indicated in Fig. 13a and b, followed by group 1 (SW, 46.5 $\mu g\,m^{-3}$), group 2 (E, 52.8 $\mu g\,m^{-3}$), group 3 (NW, 52.8 $\mu g\,m^{-3}$), and group 4 (NE, 66.1 $\mu g\,m^{-3}$) during the summer harvest; group 1 (SW, 55.7 $\mu g\,m^{-3}$), group 2 (E, 56.4 $\mu g\,m^{-3}$), group 4 (NE, 85.8 $\mu g\,m^{-3}$), and group 3 (NE, 106.8 $\mu g\,m^{-3}$) during the autumn harvest. The relatively high contribution of BBOA emerged in group 3 during the summer and autumn harvests due to the air masses from many fire locations, which is consistent with the fire location distributions around this sampling site (Fig. S1a and b). Figure S5 presents the relationship between the distribution of the mass concentrations of PM_1 species and wind direction/speed during the harvest seasons. In general, both BBOA

ACPD
14, 9109–9154, 2014

and Chl showed higher concentrations with greater wind speeds during the summer harvest, suggesting a vital role of the BB campaign around urban Nanjing in the BB pollution. However, higher BBOA and Chl concentrations were mostly associated with wind speeds of $\sim 2\,m\,s^{-1}$ during the autumn harvest, denoting the dominant role of local burning events around Nanjing.

A larger fraction of HOA and BC observed for group 2 and group 4 during the harvest seasons implies a significant contribution of primary emissions in and around the north vicinity of Nanjing to the PM pollution during the harvest seasons. HOA with high concentrations during the two harvests were associated with weak wind speeds (Fig. S5), indicating that HOA mainly came from local emissions. Overall, BC always show higher concentrations under lower and higher wind speeds (Fig. S5), denoting that the BC concentrations were associated with the local emissions and around BB campaign around urban Nanjing.

As shown in Fig. 13, the largest fraction of OOA can be found in a kind of type (the longest trajectory), such as group 2 (in the summer harvest) and group 1 (in the autumn harvest), which is also consistent with the relatively long plume transport. In addition, the relatively large fraction of NO_3 suggested a significant impact of local NO_x emissions on the PM pollution, which is also consistent with predicted plume transport from urban areas in Nanjing during the harvest seasons by the BTs. As expected, the relatively large fractions of SO_4 observed during the summer and autumn harvests are likely due to many source emissions of SO_2 from both the northwest and northeast air masses. As shown in Fig. S5, SPM (i.e. OOA, NO_3, and SO_4) almost maintained at higher levels during higher and lower wind speeds, indicating that the secondary pollutions were regional pollutants during the harvest seasons in the YRD region.

4 Conclusions

The characteristics, sources and evolution of atmospheric PM_1 species in urban Nanjing, the YRD region of China were investigated during the two harvest seasons,

ACPD
14, 9109–9154, 2014

namely the summer wheat harvest (1 to 15 June 2013) and autumn rice harvest (15 to 30 October 2013). In the summer harvest, the PM_1 loadings ranged from 3.6 to 253.0 $\mu g\,m^{-3}$ with the mean value of 38.16 $\mu g\,m^{-3}$, and was composed of OA (39 %), NO_3 (23 %), NH_4 (16 %), SO_4 (12 %), BC (8 %), and Chl (1 %); In the autumn harvest, the PM_1 loading ranged from 7.3 to 163.6 $\mu g\,m^{-3}$ witha mean value of 46.4 $\mu g\,m^{-3}$, and was composed of OA (41 %), NO_3 (20 %), NH_4 (14 %), SO_4 (11 %), BC (13 %), and Chl (1 %). OA constituted to be the largest fraction of PM_1, implying that OA plays a dominant role in the formation of high PM_1 loadings during the harvest seasons. PMF analysis resolved three OA components, i.e., HOA, BBOA, and OOA, which on average accounted for 19 % (30 %), 17 % (18 %), and 64 % (52 %) of the total OA mass concentrations during the summer (autumn) harvest, respectively. Particularly, BBOA is a main contributor to the increases of PM_1 loadings as the PM_1 loadings are larger than 100 $\mu g\,m^{-3}$. Moreover, the BBOA mass concentration correlates well with K^+, with the r^2 of 0.93 and 0.62, implying that the atmospheric K^+ loadings is a good tracer of wheat and rice straw burning during the harvests in urban Nanjing. The mass concentration of Chl correlates well with the BBOA loadings ($r^2 = 0.87$ and 0.56), implying that Chl was mainly from the BB emissions. In addition, high OOA loadings were observed during the nighttime.

The background level of f_{60} (0.26 ± 0.1 %) was determined using the f_{44} vs. f_{60} space during the non-BB periods (in July). Thus, we suggest a simpler method for on-line investigating the BBOA loadings based on the equations of BBOA = 36.7 × (m/z 60–0.26 % × OA) and = 41.4 × (m/z 60–0.26 % × OA) for the summer and autumn harvest, respectively, which correlated tightly with the BBOA loadings by the PMF method (Slope = 0.94 and r^2 = 0.98 and Slope = 1.06 and r^2 = 0.96). In addition, the f_{44} vs. f_{60} space indicates that fresh BB plumes might be transformed into aged BB plumes by a high photochemical activity. Overall, the OA mass concentration, OA fraction, and OA/ΔCO ratio increase with the increasing of the O_x loadings, respectively, during daytime, suggesting that the gas-phase oxidation might play an important role in the afternoon. Furthermore, the OA mass decreases with the aging of BB plumes, imply-

ACPD
14, 9109–9154, 2014

ing that the fresh BB plumes play a key contribution to ambient OA burden during the harvest seasons.

Combination of BTs analysis with local wind indicates that the air masses around Jiangsu province represented the most severe PM pollution, with high PM_1 mass loadings of 66.1 $\mu g\,m^{-3}$ and 106.8 $\mu g\,m^{-3}$ during the summer and autumn harvests, respectively. In addition, a large contribution of BBOA to the total PM_1 was mainly during the northeasterly and northwesterly air masses origins during the summer harvest. The northeasterly and southerly air masses displayed large PM_1 loadings with a high BBOA mass fraction during the autumn harvest. Therefore, transport processes and local emissions play an important role in the heavy pollution during the harvest seasons in Nanjing.

Supplementary material related to this article is available online at http://www.atmos-chem-phys-discuss.net/14/9109/2014/acpd-14-9109-2014-supplement.pdf.

Acknowledgements. This work was funded by the Natural Science Key Research of Jiangsu Province High Education (Grant No. 11KJA170002), the Foundation Research Project of Jiangsu Province (Grant No. BK2012884), and the Project Funded by the Jiangsu Province Science & Technology Support Program (Grant No. BE2012771). We are very grateful for the help of Douglas R. Worsnop and John T. Jayne (Aerodyne Research Inc.) concerning the ACSM measurements. We also would like to thank P. Chen (Handix LLC) and W. Li (South Coast Air Quality Management District) for providing constructive comments and help in improving the contents.

References

Andreae, M. O. and Merlet, P.: Emission of trace gases and aerosols from biomass burning, Global Biogeochem. Cy., 15, 955–966, 2001.

ACPD
14, 9109–9154, 2014

Alfarra, M. R., Prévôt, A. S. H., Szidat, S., Sandradewi, J., Weimer, S., Schreiber, D., Mohr, M., and Baltensperger, U.: Identification of the mass spectral signature of organic aerosols from wood burning emissions, Environ. Sci. Technol., 41, 5770–5777, 2007.

Aiken, A. C., DeCarlo, P. F., Kroll, J. H., Worsnop, D. R., Alex, H. J., Docherty, K. S., Ulbrich, I. M., Mohr, C., Kimmel, J. R., Sueper, D., Sun, Y. L., Zhang, Q., Trimborn. A., Northway, M., Ziemann, P. J., Canagaratna, M. R., Onasch, T. B., Alfarra, R., Prévôt, A. S. H., Dommen, J., Duplissy, J., Metzger, A., Baltensperger, U., and Jimenez, J. L.: O/C and OM/OC ratios of primary, secondary, and ambient organic aerosols with high-resolution time-of-flight aerosol mass spectrometry, Environ. Sci. Technol., 42, 4478–4485, 2008.

Aiken, A. C., Salcedo, D., Cubison, M. J., Huffman, J. A., DeCarlo, P. F., Ulbrich, I. M., Docherty, K. S., Sueper, D., Kimmel, J. R., Worsnop, D. R., Trimborn, A., Northway, M., Stone, E. A., Schauer, J. J., Volkamer, R. M., Fortner, E., de Foy, B., Wang, J., Laskin, A., Shutthanandan, V., Zheng, J., Zhang, R., Gaffney, J., Marley, N. A., Paredes-Miranda, G., Arnott, W. P., Molina, L. T., Sosa, G., and Jimenez, J. L.: Mexico City aerosol analysis during MILAGRO using high resolution aerosol mass spectrometry at the urban supersite (T0) – Part 1: Fine particle composition and organic source apportionment, Atmos. Chem. Phys., 9, 6633–6653, doi:10.5194/acp-9-6633-2009, 2009.

Aiken, A. C., de Foy, B., Wiedinmyer, C., DeCarlo, P. F., Ulbrich, I. M., Wehrli, M. N., Szidat, S., Prevot, A. S. H., Noda, J., Wacker, L., Volkamer, R., Fortner, E., Wang, J., Laskin, A., Shutthanandan, V., Zheng, J., Zhang, R., Paredes-Miranda, G., Arnott, W. P., Molina, L. T., Sosa, G., Querol, X., and Jimenez, J. L.: Mexico city aerosol analysis during MILAGRO using high resolution aerosol mass spectrometry at the urban supersite (T0) – Part 2: Analysis of the biomass burning contribution and the non-fossil carbon fraction, Atmos. Chem. Phys., 10, 5315–5341, doi:10.5194/acp-10-5315-2010, 2010.

Allan, J. D., Bower, K. N., Coe, H., Boudries, H., Jayne, J. T., Canagaratna, M. R., Millet, D. B., Goldstein, A. H., Quinn, P. K., and Weber, R. J., W. D. R.: Submicron aerosol composition at Trinidad Head, California, during ITCT 2K2: its relationship with gas phase volatile organic carbon and assessment of instrument performance, J. Geophys. Res., 109, D23S24, doi:10.1029/2003JD004208, 2004.

Allan, J. D., Williams, P. I., Morgan, W. T., Martin, C. L., Flynn, M. J., Lee, J., Nemitz, E., Phillips, G. J., Gallagher, M. W., and Coe, H.: Contributions from transport, solid fuel burning and cooking to primary organic aerosols in two UK cities, Atmos. Chem. Phys., 10, 647–668, doi:10.5194/acp-10-647-2010, 2010.

ACPD
14, 9109–9154, 2014

Bougiatioti, A., Stavroulas, I., Kostenidou, E., Zarmpas, P., Theodosi, C., Kouvarakis, G., Canonaco, F., Prévôt, A. S. H., Nenes, A., Pandis, S. N., and Mihalopoulos, N.: Processing of biomass burning aerosol in the Eastern Mediterranean during summertime, Atmos. Chem. Phys. Discuss., 13, 25969–25999, doi:10.5194/acpd-13-25969-2013, 2013.

Canagaratna, M., Jayne, J., Jimenez, J. L., Allan, J. A., Alfarra, R., Zhang, Q., Onasch, T., Drewnick, F., Coe, H., Middlebrook, A., Delia, A., Williams, L., Trimborn, A., Northway, M., Kolb, C., Davidovits, P., and Worsnop, D.: Chemical and microphysical characterization of aerosols via Aerosol Mass Spectrometry, Mass Spectrom. Rev., 26, 185–222, 2007.

Chebbi, A. and Carlier, P.: Carboxylic acids in the troposphere, occurrence, sources, and sinks: a review, Atmos. Environ., 30, 4233–4249, 1996.

Cheng, Y., Engling, G., He, K.-B., Duan, F.-K., Ma, Y.-L., Du, Z.-Y., Liu, J.-M., Zheng, M., and Weber, R. J.: Biomass burning contribution to Beijing aerosol, Atmos. Chem. Phys., 13, 7765–7781, doi:10.5194/acp-13-7765-2013, 2013.

Crippa, M., DeCarlo, P. F., Slowik, J. G., Mohr, C., Heringa, M. F., Chirico, R., Poulain, L., Freutel, F., Sciare, J., Cozic, J., Di Marco, C. F., Elsasser, M., Nicolas, J. B., Marchand, N., Abidi, E., Wiedensohler, A., Drewnick, F., Schneider, J., Borrmann, S., Nemitz, E., Zimmermann, R., Jaffrezo, J.-L., Prévôt, A. S. H., and Baltensperger, U.: Wintertime aerosol chemical composition and source apportionment of the organic fraction in the metropolitan area of Paris, Atmos. Chem. Phys., 13, 961–981, doi:10.5194/acp-13-961-2013, 2013a.

Crippa, M., Canonaco, F., Lanz, V. A., Äijälä, M., Allan, J. D., Carbone, S., Capes, G., Dall'Osto, M., Day, D. A., DeCarlo, P. F., Di Marco, C. F., Ehn, M., Eriksson, A., Freney, E., Hildebrandt Ruiz, L., Hillamo, R., Jimenez, J.-L., Junninen, H., Kiendler-Scharr, A., Kortelainen, A.-M., Kulmala, M., Mensah, A. A., Mohr, C., Nemitz, E., O'Dowd, C., Ovadnevaite, J., Pandis, S. N., Petäjä, T., Poulain, L., Saarikoski, S., Sellegri, K., Swietlicki, E., Tiitta, P., Worsnop, D. R., Baltensperger, U., and Prévôt, A. S. H.: Organic aerosol components derived from 25 AMS datasets across Europe using a newly developed ME-2 based source apportionment strategy, Atmos. Chem. Phys. Discuss., 13, 23325–23371, doi:10.5194/acpd-13-23325-2013, 2013b.

Cubison, M. J., Ortega, A. M., Hayes, P. L., Farmer, D. K., Day, D., Lechner, M. J., Brune, W. H., Apel, E., Diskin, G. S., Fisher, J. A., Fuelberg, H. E., Hecobian, A., Knapp, D. J., Mikoviny, T., Riemer, D., Sachse, G. W., Sessions, W., Weber, R. J., Weinheimer, A. J., Wisthaler, A., and Jimenez, J. L.: Effects of aging on organic aerosol from open biomass burning smoke in

ACPD
14, 9109–9154, 2014

aircraft and laboratory studies, Atmos. Chem. Phys., 11, 12049–12064, doi:10.5194/acp-11-12049-2011, 2011.

DeCarlo, P. F., Dunlea, E. J., Kimmel, J. R., Aiken, A. C., Sueper, D., Crounse, J., Wennberg, P. O., Emmons, L., Shinozuka, Y., Clarke, A., Zhou, J., Tomlinson, J., Collins, D. R., Knapp, D., Weinheimer, A. J., Montzka, D. D., Campos, T., and Jimenez, J. L.: Fast airborne aerosol size and chemistry measurements above Mexico City and Central Mexico during the MILAGRO campaign, Atmos. Chem. Phys., 8, 4027–4048, doi:10.5194/acp-8-4027-2008, 2008.

DeCarlo, P. F., Ulbrich, I. M., Crounse, J., de Foy, B., Dunlea, E. J., Aiken, A. C., Knapp, D., Weinheimer, A. J., Campos, T., Wennberg, P. O., and Jimenez, J. L.: Investigation of the sources and processing of organic aerosol over the Central Mexican Plateau from aircraft measurements during MILAGRO, Atmos. Chem. Phys., 10, 5257–5280, doi:10.5194/acp-10-5257-2010, 2010.

de Gouw, J. A., Middlebrook, A. M., Warneke, C., Goldan, P. D., Kuster, W. C., Roberts, J. M., Fehsenfeld, F. C., Worsnop, D. R., Canagaratna, M. R., Pszenny, A. A. P., Keene, W. C., Marchewka, M., Bertman, S. B., and Bates, T. S.: Budget of organic carbon in a polluted atmosphere: results from the New England Air Quality Study in 2002, J. Geophys. Res. Atmos., 110, D16305, doi:10.1029/2004JD005623, 2005.

Ding, A. J., Fu, C. B., Yang, X. Q., Sun, J. N., Petäjä, T., Kerminen, V.-M., Wang, T., Xie, Y., Herrmann, E., Zheng, L. F., Nie, W., Liu, Q., Wei, X. L., and Kulmala, M.: Intense atmospheric pollution modifies weather: a case of mixed biomass burning with fossil fuel combustion pollution in eastern China, Atmos. Chem. Phys., 13, 10545–10554, doi:10.5194/acp-13-10545-2013, 2013.

Draxler, R. R. and Rolph, G. D.: HYSPLIT (HYbrid Single-Particle Lagrangian Integrated Trajectory) Model Access via NOAA ARL READY Website, NOAA Air Resources Laboratory, Silver Spring, MD, available at: http://www.arl.noaa.gov/ready/hysplit4.html (last access: November 2013), 2003.

Du, H. H., Kong, L. D., Cheng, T. T., Chen, J. M., Du, J. F., Li, L., Xia, X. G., Leng, C. P., and Huang, G. H.: Insights into summertime haze pollution events over Shanghai based on online water-soluble ionic composition of aerosols, Atmos. Environ., 45, 5131–5137, 2011.

Ge, W. Z., Chen, R. J., Song, W. M., and Kan, H. D.: Daily Visibility and Hospital Admission in Shanghai, China, Biomed. Environ. Sci., 24, 117–121, 2011.

ACPD
14, 9109–9154, 2014

Gilardoni, S., Liu, S., Takahama, S., Russell, L. M., Allan, J. D., Steinbrecher, R., Jimenez, J. L., De Carlo, P. F., Dunlea, E. J., and Baumgardner, D.: Characterization of organic ambient aerosol during MIRAGE 2006 on three platforms, Atmos. Chem. Phys., 9, 5417–5432, doi:10.5194/acp-9-5417-2009, 2009.

He, L.-Y., Lin, Y., Huang, X.-F., Guo, S., Xue, L., Su, Q., Hu, M., Luan, S.-J., and Zhang, Y.-H.: Characterization of high-resolution aerosol mass spectra of primary organic aerosol emissions from Chinese cooking and biomass burning, Atmos. Chem. Phys., 10, 11535–11543, doi:10.5194/acp-10-11535-2010, 2010.

Heringa, M. F., DeCarlo, P. F., Chirico, R., Tritscher, T., Dommen, J., Weingartner, E., Richter, R., Wehrle, G., Prévôt, A. S. H., and Baltensperger, U.: Investigations of primary and secondary particulate matter of different wood combustion appliances with a high-resolution time-of-flight aerosol mass spectrometer, Atmos. Chem. Phys., 11, 5945–5957, doi:10.5194/acp-11-5945-2011, 2011.

Hu, W. W., Hu, M., Yuan, B., Jimenez, J. L., Tang, Q., Peng, J. F., Hu, W., Shao, M., Wang, M., Zeng, L. M., Wu, Y. S., Gong, Z. H., Huang, X. F., and He, L. Y.: Insights on organic aerosol aging and the influence of coal combustion at a regional receptor site of central eastern China, Atmos. Chem. Phys., 13, 10095–10112, doi:10.5194/acp-13-10095-2013, 2013.

Huang, X.-F., He, L.-Y., Hu, M., Canagaratna, M. R., Kroll, J. H., Ng, N. L., Zhang, Y.-H., Lin, Y., Xue, L., Sun, T.-L., Liu, X.-G., Shao, M., Jayne, J. T., and Worsnop, D. R.: Characterization of submicron aerosols at a rural site in Pearl River Delta of China using an Aerodyne High-Resolution Aerosol Mass Spectrometer, Atmos. Chem. Phys., 11, 1865–1877, doi:10.5194/acp-11-1865-2011, 2011.

Huang, X.-F., He, L.-Y., Xue, L., Sun, T.-L., Zeng, L.-W., Gong, Z.-H., Hu, M., and Zhu, T.: Highly time-resolved chemical characterization of atmospheric fine particles during 2010 Shanghai World Expo, Atmos. Chem. Phys., 12, 4897–4907, doi:10.5194/acp-12-4897-2012, 2012.

Jimenez, J. L., Canagaratna, M. R., Donahue, N. M., Prévôt, A. S. H., Zhang, Q., Kroll, J. H., DeCarlo, P. F., Allan, J. D., Coe, H., Ng, N. L., Aiken, A. C., Docherty, K. S., Ulbrich, I. M., Grieshop, A. P., Robinson, A. L., Duplissy, J., Smith, J. D., Wilson, K. R., Lanz, V. A., Hueglin, C., Sun, Y. L., Tian, J., Laaksonen, A., Raatikainen, T., Rautiainen, J., Vaattovaara, P., Ehn, M., Kulmala, M., Tomlinson, J. M., Collins, D. R., Cubison, M. J. E., Dunlea, J., Huffman, J. A., Onasch, T. B., Alfarra, M. R., Williams, P. I., Bower, K., Kondo, Y., Schneider, J., Drewnick, F., Borrmann, S., Weimer, S., Demerjian, K., Salcedo, D., Cottrell, L., Griffin, R., Takami, A., Miyoshi, T., Hatakeyama, S., Shimono, A., Sun, J. Y.,

ACPD
14, 9109–9154, 2014

Zhang, Y. M., Dzepina, K., Kimmel, J. R., Sueper, D., Jayne, J. T., Herndon, S. C., Trimborn, A. M., Williams, L. R., Wood, E. C., Middlebrook, A. M., Kolb, C. E., Baltensperger, U., and Worsnop, D. R.: Evolution of organic aerosols in the atmosphere, Science, 326, 1525–1529, 2009.

Jolleys, M. D., Coe, H., McFiggans, G., Capes, G., Allan, J. D., Crosier, J., Williams, P. I., Allen, G., Bower, K. N., Jimenez, J. L., Russell, L. M., Grutter, M., and Baumgardner, D.: Characterizing the aging of biomass burning organic aerosol by use of mixing ratios: a meta-analysis of four regions, Environ. Sci. Technol., 46, 13093–13102, 2012.

Justice, C. O., Giglio, L., Korontzi, S., Owens, J., Morisette, J. T., Roy, D., Descloitres, J., Alleaume, S., Petitcolin, F., and Kaufman, Y.: The MODIS fire products, Remote Sens. Environ., 83, 244–262, 2002.

Kaufman, Y. J., Tanre, D., and Boucher, O.: A satellite view of aerosols in the climate system, Nature, 419, 215–23, 2002.

Kaufman, Y. J., Ichoku, C., Giglio, L., Korontzi, S., Chu, D. A., Hao, W. M., Li, R. R., Justice, C. O.: Fire and smoke observed from the earth observing system MODIS instrument-products, validation, and operational use, Int. J. Remote Sens., 24, 1765–781, 2003.

Kroll, J. H., Donahue, N. M., Jimenez, J. L., Kessler, S. H., Canagaratna, M. R., Wilson, K. R., Altieri, K. E., Mazzoleni, L. R., Wozniak, A. S., Bluhm, H., Mysak, E. R., Smith, J. D., Kolb, C. E., and Worsnop, D. R.: Carbon oxidation state as a metric for describing the chemistry of atmospheric organic aerosol, Nature Chem., 3, 133–139, 2011.

Lanz, V. A., Alfarra, M. R., Baltensperger, U., Buchmann, B., Hueglin, C., and Prévôt, A. S. H.: Source apportionment of submicron organic aerosols at an urban site by factor analytical modelling of aerosol mass spectra, Atmos. Chem. Phys., 7, 1503–1522, doi:10.5194/acp-7-1503-2007, 2007.

Lanz, V. A., Prévôt, A. S. H., Alfarra, M. R., Weimer, S., Mohr, C., DeCarlo, P. F., Gianini, M. F. D., Hueglin, C., Schneider, J., Favez, O., D'Anna, B., George, C., and Baltensperger, U.: Characterization of aerosol chemical composition with aerosol mass spectrometry in Central Europe: an overview, Atmos. Chem. Phys., 10, 10453–10471, doi:10.5194/acp-10-10453-2010, 2010.

Lee, T., Sullivan, A. P., Mack, L., Jimenez, J. L., Kreidenweis, S. M., Onasch, T. B., Worsnop, D. R., Malm, W., Wold, C. E., Hao, W. M., and Collett, J. L.: Chemical smoke marker emissions during flaming and smoldering phases of laboratory open burning of wildland fuels, Aerosol Sci. Tech., 44, 1–5, 2010.

ACPD
14, 9109–9154, 2014

Li, H. Y., Han, Z. W., and Cheng, T. T.: Agricultural fire impacts on the air quality of Shanghai during summer harvest time, Aerosol Air Qual. Res., 10, 95–101, 2010.
Li, X. H., Wang, S. X., Duan, L., Hao, J. M., Li, Y. S., and Yang, L.: Particulate and trace gas emissions from open burning of wheat straw and corn stover in China, Environ. Sci. Technol., 41, 6052–6058, 2007.
Li, Y. J., Lee, B. Y. L., Yu, J. Z., Ng, N. L., and Chan, C. K.: Evaluating the degree of oxygenation of organic aerosol during foggy and hazy days in Hong Kong using high-resolution time-of-flight aerosol mass spectrometry (HR-ToF-AMS), Atmos. Chem. Phys., 13, 8739–8753, doi:10.5194/acp-13-8739-2013, 2013.
Liu, D., Allan, J., Corris, B., Flynn, M., Andrews, E., Ogren, J., Beswick, K., Bower, K., Burgess, R., Choularton, T., Dorsey, J., Morgan, W., Williams, P. I., and Coe, H.: Carbonaceous aerosols contributed by traffic and solid fuel burning at a polluted rural site in Northwestern England, Atmos. Chem. Phys., 11, 1603–1619, doi:10.5194/acp-11-1603-2011, 2011.
Maenhaut, W., Vermeylen, R., Claeys, M., Vercauteren, J., Matheeussen, C., Roekens, E.: Assessment of the contribution from wood burning to the PM_{10} aerosol in Flanders, Belgium, Sci. Total Environ., 437, 226–236, 2012.
Middlebrook, A. M., Bahreini, R., Jimenez, J. L., and Canagaratna, M. R.: Evaluation of composition-dependent collection efficiencies for the aerodyne aerosol mass spectrometer using field data, Aerosol Sci. Tech., 46, 258–271, 2011.
Mohr, C., DeCarlo, P. F., Heringa, M. F., Chirico, R., Slowik, J. G., Richter, R., Reche, C., Alastuey, A., Querol, X., Seco, R., Peñuelas, J., Jiménez, J. L., Crippa, M., Zimmermann, R., Baltensperger, U., and Prévôt, A. S. H.: Identification and quantification of organic aerosol from cooking and other sources in Barcelona using aerosol mass spectrometer data, Atmos. Chem. Phys., 12, 1649–1665, doi:10.5194/acp-12-1649-2012, 2012.
Ng, N. L., Canagaratna, M. R., Zhang, Q., Jimenez, J. L., Tian, J., Ulbrich, I. M., Kroll, J. H., Docherty, K. S., Chhabra, P. S., Bahreini, R., Murphy, S. M., Seinfeld, J. H., Hildebrandt, L., Donahue, N. M., DeCarlo, P. F., Lanz, V. A., Prévôt, A. S. H., Dinar, E., Rudich, Y., and Worsnop, D. R.: Organic aerosol components observed in Northern Hemispheric datasets from Aerosol Mass Spectrometry, Atmos. Chem. Phys., 10, 4625–4641, doi:10.5194/acp-10-4625-2010, 2010.
Ng, N. L., Herndon, S. C., Trimborn, A., Canagaratna, M. R., Croteau, P. L., Onasch, T. B., Sueper, D., Worsnop, D. R., Zhang, Q., Sun, Y. L., and Jayne, J. T.: An Aerosol Chemical

ACPD
14, 9109–9154, 2014

Speciation Monitor (ACSM) for routine monitoring of the composition and mass concentrations of ambient aerosol, Aerosol Sci. Tech., 45, 7, 770–784, 2011a.
Ng, N. L., Canagaratna, M. R., Jimenez, J. L., Chhabra, P. S., Seinfeld, J. H., and Worsnop, D. R.: Changes in organic aerosol composition with aging inferred from aerosol mass spectra, Atmos. Chem. Phys., 11, 6465–6474, doi:10.5194/acp-11-6465-2011, 2011b.
Ng, N. L., Canagaratna, M. R., Jimenez, J. L., Zhang, Q., Ulbrich, I. M., and Worsnop, D. R.: Real-time methods for estimating organic component mass concentrations from aerosol mass spectrometer data, Environ. Sci. Technol., 45, 910–916, 2011c.
Paatero, P.: Least squares formulation of robust non-negative factor analysis, Chemom. Intell. Lab. Syst., 37, 23–35, 1997.
Paatero, P. and Tapper, U.: Positive matrix factorization: a non-negative factor model with optimal utilization of error estimates of data values, Environmetrics, 5, 111–126, 1994.
Ramanathan, V., Crutzen, P. J, Kiehl, J. T., and Rosenfeld, D.: Atmosphere, aerosols, climate, and the hydrological cycle, Science, 294, 2119–2124, 2001.
Reche, C., Viana, M., Amato, F., Alastuey, A., Moreno, T., Hillamo, R., Teinila, K., Saarnio, K., Seco, R., Penuelas, J., Mohr, C., Prévôt, A. S. H., and Querol, X,.: Biomass burning contributions to urban aerosols in a coastal Mediterranean City, Sci. Total Environ., 427, 175–190, 2012.
Saleh, R., Hennigan, C. J., McMeeking, G. R., Chuang, W. K., Robinson, E. S., Coe, H., Donahue, N. M., and Robinson, A. L.: Absorptivity of brown carbon in fresh and photo-chemically aged biomass-burning emissions, Atmos. Chem. Phys., 13, 7683–7693, doi:10.5194/acp-13-7683-2013, 2013.
Sullivan, A. P., Holden, A. S., Patterson, L. A., McMeeking, G. R., Kreidenweis, S. M., Malm, W. C., Hao, W. M., Wold, C. E., and Collett Jr., J. L.: A method for smoke marker measurements and its potential application for determining the contribution of biomass burning from wildfires and prescribed fires to ambient $PM_{2.5}$ organic carbon, J. Geophys. Res., 113, D22302, doi:10.1029/2008JD010216, 2008.
Sun, Y. L., Zhang, Q., Schwab, J. J., Chen, W. N., Bae, M. S., Lin, Y. C., Hung, H. M., and Demerjian, K. L.: A case study of aerosol processing and evolution in summer in New York City, Atmos. Chem. Phys., 11, 12737–12750, doi:10.5194/acp-11-12737-2011, 2011.
Sun, Y. L., Wang, Z. F., Dong, H. B., Yang, T., Li, J., Pan, X. L., Chen, P., and Jayne, J. T.: Characterization of summer organic and inorganic aerosols in Beijing, China with an Aerosol Chemical Speciation Monitor, Atmos. Environ., 51, 250–259, 2012a.

ACPD
14, 9109–9154, 2014

Sun, Y. L., Zhang, Q., Schwab, J. J., Yang, T., Ng, N. L., and Demerjian, K. L.: Factor analysis of combined organic and inorganic aerosol mass spectra from high resolution aerosol mass spectrometer measurements, Atmos. Chem. Phys., 12, 8537–8551, doi:10.5194/acp-12-8537-2012, 2012b.

Sun, Y. L., Wang, Z. F., Fu, P. Q., Yang, T., Jiang, Q., Dong, H. B., Li, J., and Jia, J. J.: Aerosol composition, sources and processes during wintertime in Beijing, China, Atmos. Chem. Phys., 13, 4577–4592, doi:10.5194/acp-13-4577-2013, 2013a.

Sun, Y. L., Wang, Z. F., Fu, P. Q., Jiang, Q., Yang, T., Li, J., and Ge, X. L.: The impact of relative humidity on aerosol composition and evolution processes during wintertime in Beijing, China, Atmos. Environ., 77, 927–934, 2013b.

Takegawa, N., Miyakawa, T., Kondo, Y., Jimenez, J. L., Zhang, Q., Worsnop, D. R., and Fukuda, M.: Seasonal and diurnal variations of submicron organic aerosol in Tokyo observed using the Aerodyne aerosol mass spectrometer, J. Geophys. Res., 111, D11206, doi:10.1029/2005JD006515, 2006.

Ulbrich, I. M., Canagaratna, M. R., Zhang, Q., Worsnop, D. R., and Jimenez, J. L.: Interpretation of organic components from Positive Matrix Factorization of aerosol mass spectrometric data, Atmos. Chem. Phys., 9, 2891–2918, doi:10.5194/acp-9-2891-2009, 2009.

Wang, G. H., Kawamura, K., Xie, M. J., Hu, S. Y., Cao, J. J., An, Z. H., Waston, J. G., and Chow, J. C.: Organic molecular compositions and size distributions of chinese summer and autumn aerosols from Nanjing: characteristic haze event caused by wheat straw burning, Environ. Sci. Technol., 43, 6493–6499, 2009a.

Wang, Y. Q., Zhang, X. Y., and Draxler, R. R.: TrajStat: GIS-based software that uses various trajectory statistical analysis methods to identify potential sources from long-term air pollution measurement data, Environ. Modell. Softw., 24, 938–939, 2009b.

Watson, J. G.: Visibility: science and regulation, J. Air Waste Manage. Assoc., 52, 628–713, 2002.

Xiao, R., Takegawa, N., Zheng, M., Kondo, Y., Miyazaki, Y., Miyakawa, T., Hu, M., Shao, M., Zeng, L., Gong, Y., Lu, K., Deng, Z., Zhao, Y., and Zhang, Y. H.: Characterization and source apportionment of submicron aerosol with aerosol mass spectrometer during the PRIDE-PRD 2006 campaign, Atmos. Chem. Phys., 11, 6911–6929, doi:10.5194/acp-11-6911-2011, 2011.

ACPD
14, 9109–9154, 2014

Zhang, H., Ye, X., Cheng, T., Chen, J., Yang, X., Wang, L., Zhang, R.: A laboratory study of agricultural crop residue combustion in China: emission factors and emission inventory, Atmos. Environ., 42, 8432–8441, 2008.

Zhang, Q., Worsnop, D. R., Canagaratna, M. R., and Jimenez, J. L.: Hydrocarbon-like and oxygenated organic aerosols in Pittsburgh: insights into sources and processes of organic aerosols, Atmos. Chem. Phys., 5, 3289–3311, doi:10.5194/acp-5-3289-2005, 2005a.

Zhang, Q., Alfarra, M. R., Worsnop, D., Allan, J. D., Coe, H., Cangaratna, M. R., Jimenez, J. L.: Deconvolution and quantification of hydrocarbon-like and oxygenated organic aerosols based on aerosol mass spectrometry, Environ. Sci. Technol., 39, 4938–4952, 2005b.

Zhang, Q., Jimenez, J. L., Canagaratna, M. R., Allan, J. D., Coe, H., Ulbrich, I. M., Alfarra, M. R., Takami, A., Middlebrook, A. M., Sun, Y. L., Dzepina, K., Dunlea, E., Docherty, K., DeCarlo, P, F., Salcedo, D., Onasch, T., Jayne, J. T., Miyoshi, T., Shimono, A., Hatakeyama, S., Takegawa, N., Kondo, Y., Schneider, J., Drewnick, F., Borrmann, S., Weimer, S., Demerjian, K., Williams, P., Bower, K., Bahreini, R., Cottrell, L., Griffin, R. J., Rautiainen, J., Sun, J. Y., Zhang, Y. M., Worsnop, D. R.: Ubiquity and dominance of oxygenated species in organic aerosols in anthropogenically-influenced Northern Hemisphere midlatitudes, Geophys. Res. Lett., 34, L13801, doi:10.1029/2007GL029979, 2007.

Zhang, Q., Jimenez, J. L., Canagaratna, M. R., Ulbrich, I. M., Ng, N. L., Worsnop, D. R., Sun, Y. L.: Understanding atmospheric organic aerosols via factor analysis of aerosol mass spectrometry: a review, Anal. Bioanal. Chem., 401, 3045–3067, 2011.

ACPD
14, 9109–9154, 2014

Table 1. Mean mass concentration of PM_1 (NR-PM_1 + BC) ($\mu g\,m^{-3}$) and standard deviation (S.D.) during the harvest seasons.

Species	Summer harvest		Autumn harvest		Entire harvest seasons	
	Mean	S.D.	Mean	S.D.	Mean	S.D.
NO_3	9.0	7.1	9.2	6.2	9.1	7.0
SO_4	5.0	2.4	4.7	2.5	4.8	2.4
NH_4	7.0	3.5	6.4	3.5	6.5	3.5
Chl	0.4	0.9	0.7	0.8	0.6	0.9
OA	15.4	12.8	22.3	17.5	18.8	15.7
BC	3.2	2.2	6.0	3.8	4.6	3.4
PM_1	38.5	24.3	46.4	27.0	42.3	26.0
HOA	2.7	2.4	5.7	8.4	4.2	6.3
BBOA	2.4	3.7	3.5	5.9	3.0	4.0
OOA	9.1	6.7	10.1	5.5	9.6	6.2

ACPD
14, 9109–9154, 2014

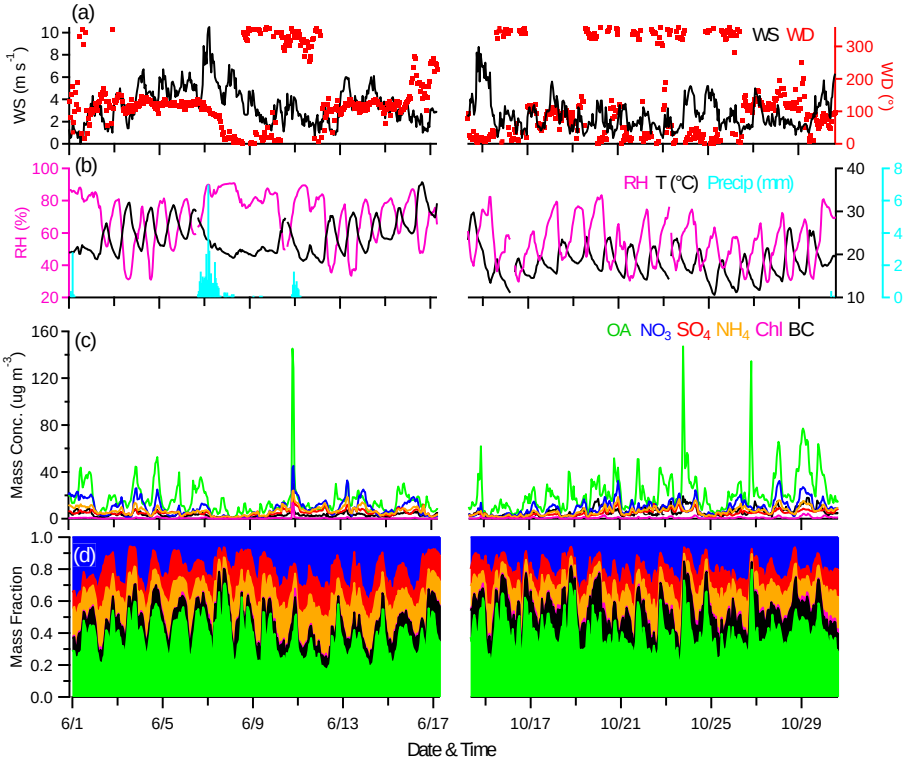

Fig. 1. Time series of **(a)** wind speed (WS) and wind direction (WD), **(b)** relative humidity (RH), temperature (T) and precipitation, **(c)** submicron aerosol species, i.e., organic aerosol (OA), ammonium (NH_4), nitrate (NO_3), sulfate (SO_4), chloride (Chl) and black carbon (BC), and **(d)** mass fraction during the harvest seasons.

ACPD
14, 9109–9154, 2014

Submicron aerosols during harvest seasons

Y. J. Zhang et al.

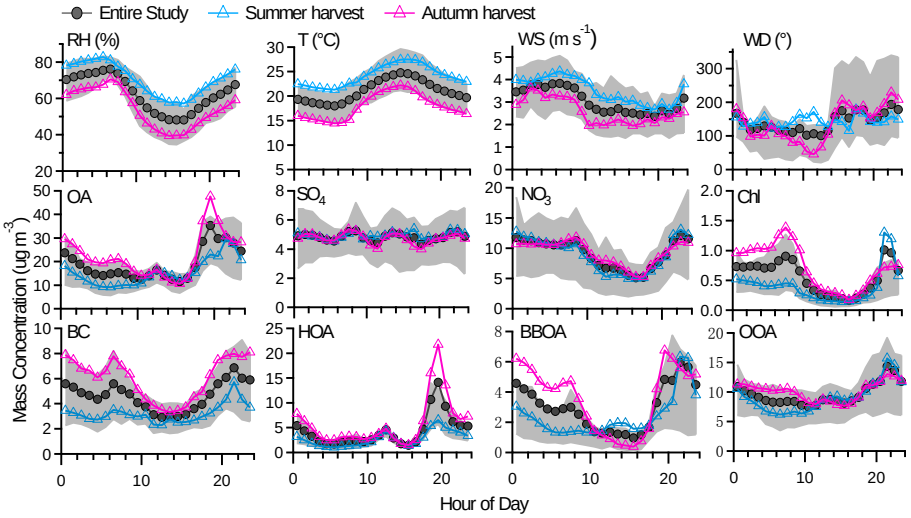

Fig. 2. Diurnal variation patterns of meteorological factors (i.e., RH, T, WS, and WD), PM_1 species (OA, NO_3, SO_4, Chl, and BC), and OA components (HOA, BBOA, and OOA) during the harvest seasons. The gray shaded areas indicate the 75th and 25th percentile.

ACPD
14, 9109–9154, 2014

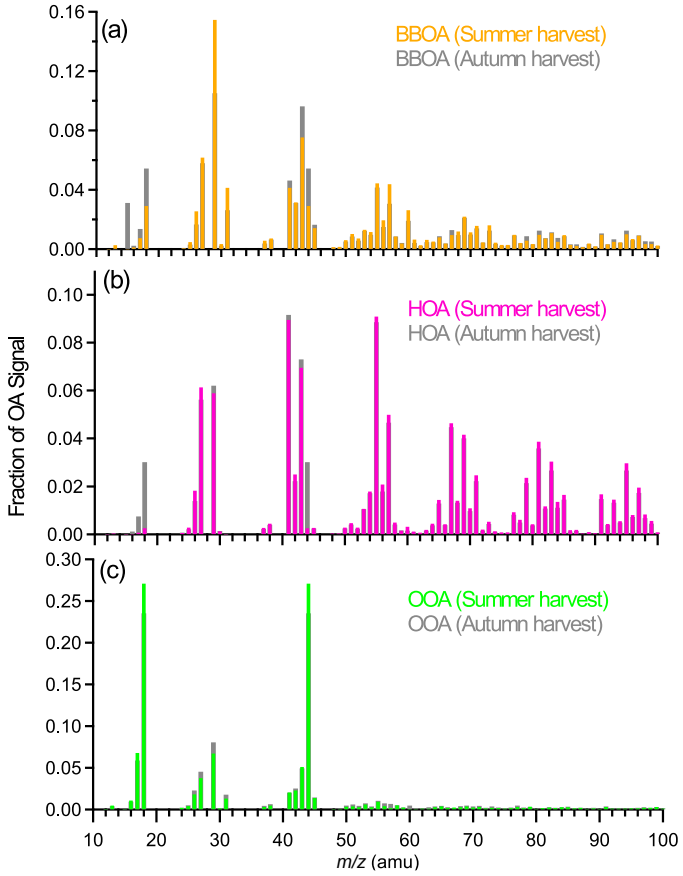

Fig. 3. Mass spectra profiles of **(a)** BBOA, **(b)** HOA, and **(c)** OOA.

ACPD
14, 9109–9154, 2014

Submicron aerosols during harvest seasons

Y. J. Zhang et al.

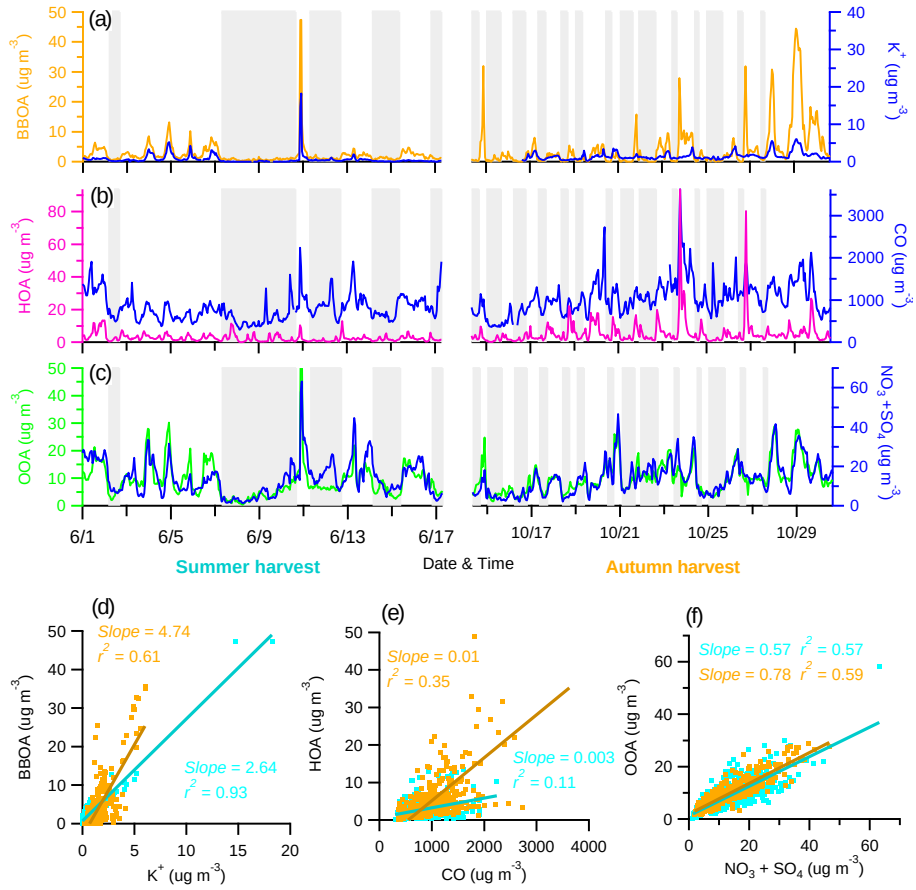

Fig. 4. Time series of **(a–c)** organic components and relevant tracer species, correlation plots of **(d)** BBOA vs. K^+, **(e)** HOA vs. CO, and **(f)** OOA vs. the sum of NO_3 and SO_4, during the summer and autumn harvests. The no/negligible biomass burning (Non-BB) periods are marked as gray shaded areas.

ACPD
14, 9109–9154, 2014

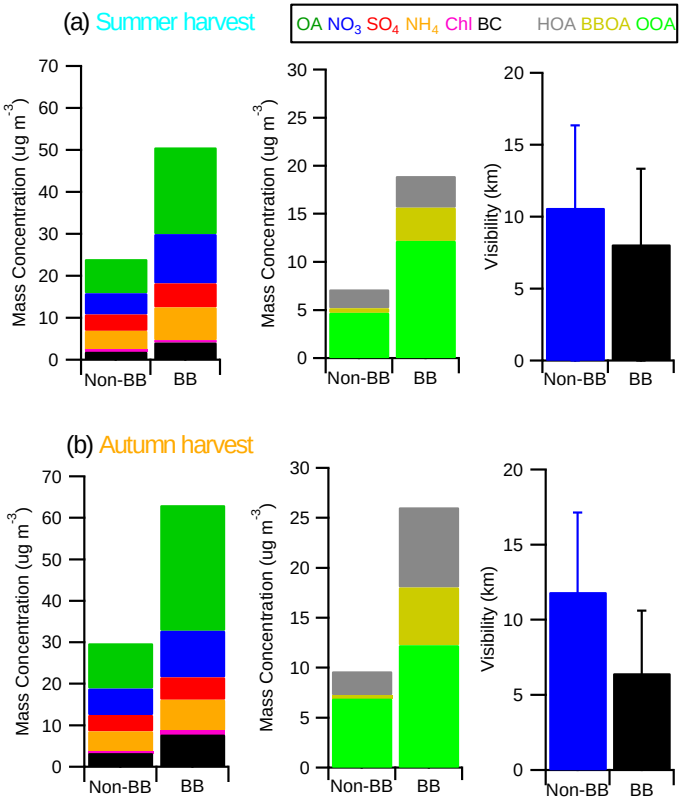

Fig. 5. Variations The composition of PM_1 species, OA sources and atmospheric visibility during no/negligible biomass burning (Non-BB) and biomass burning (BB) periods in **(a)** summer and **(b)** harvest seasons, respectively. Non-BB periods marked in Fig. 4 with gray shaded areas.

ACPD
14, 9109–9154, 2014

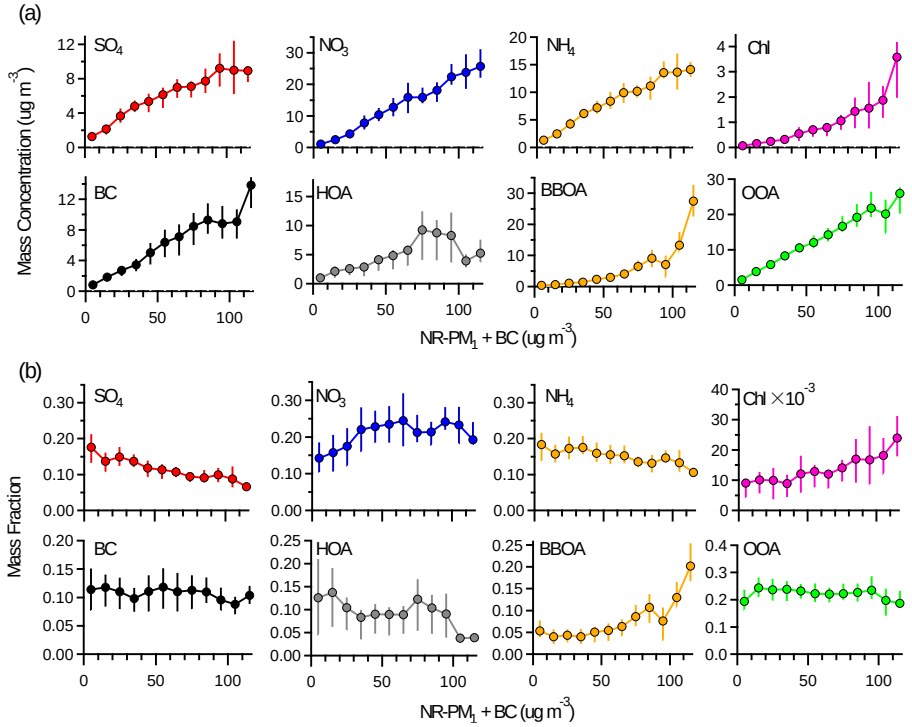

Fig. 6. Variations of **(a)** mass concentrations of PM_1 species and OA components, i.e., SO_4, NO_3, NH_4, Chl, BC, HOA, BBOA, and OOA; and **(b)** mass fractions of PM_1 species and OA components as a function of PM_1 (NR-PM_1 + BC) mass concentration. The upper and lower boundaries of lines are the 75th and 25th percentiles; and the cross symbols represent the means.

ACPD
14, 9109–9154, 2014

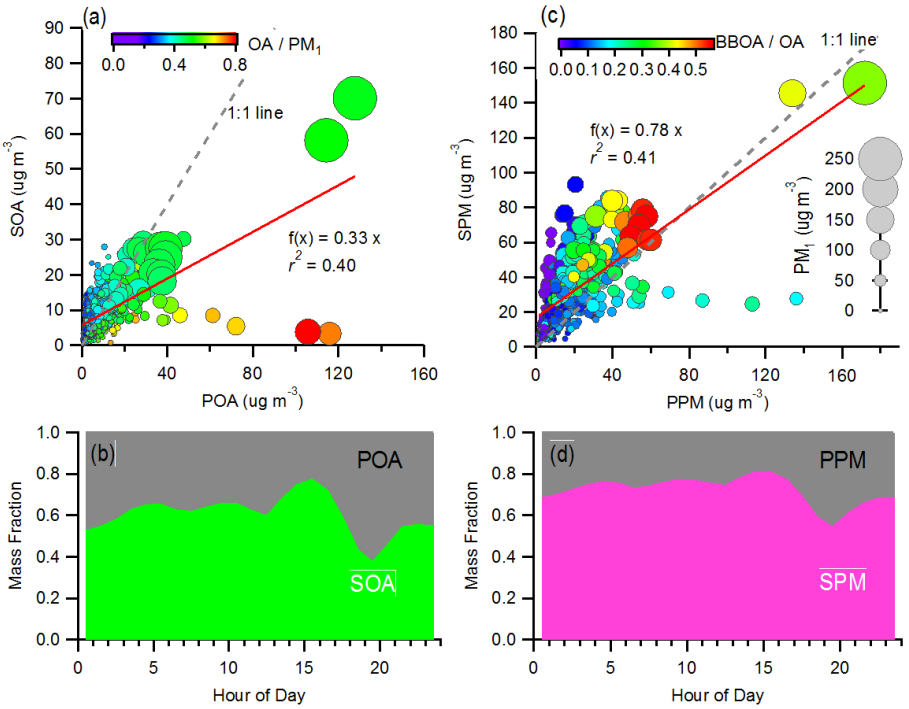

Fig. 7. Relationships between the mass concentrations of **(a)** SOA (SOA = OOA) and POA (POA = HOA + BBOA); **(b)** SPM (SPM = SOA + NO_3 + SO_4 + NH_4) and PPM (PPM = POA + BC); the diurnal plots of mass fraction of **(c)** POA vs. SOA and **(d)** PPM vs. SPM. The data colored by the mass fraction of OA in the PM_1 mass loadings. The data are sized by the PM_1 mass loadings.

ACPD
14, 9109–9154, 2014

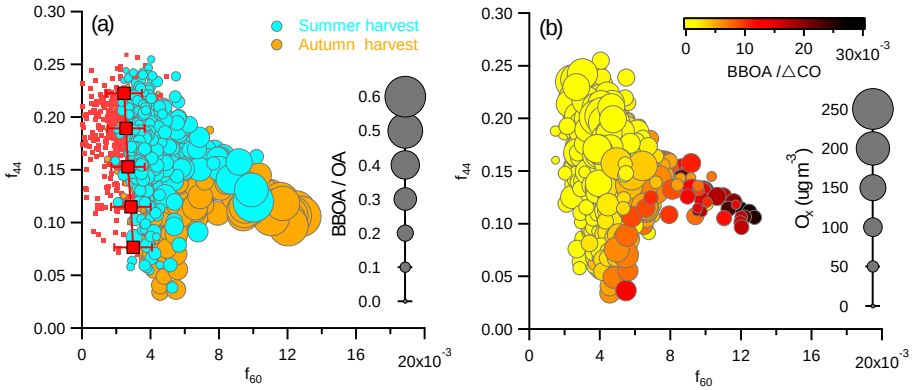

Fig. 8. Summary plots showing f_{44} vs. f_{60} for the harvest seasons: **(a)** colored by the summer and autumn harvests, respectively. Sized proportional to the ratios of BBOA/OA. Note that red dots present the background levels of f_{60}; **(b)** colored by the ratios of BBOA/ΔCO and sized proportional to O_x ($O_x = O_3 + NO_2$) mass loadings.

ACPD
14, 9109–9154, 2014

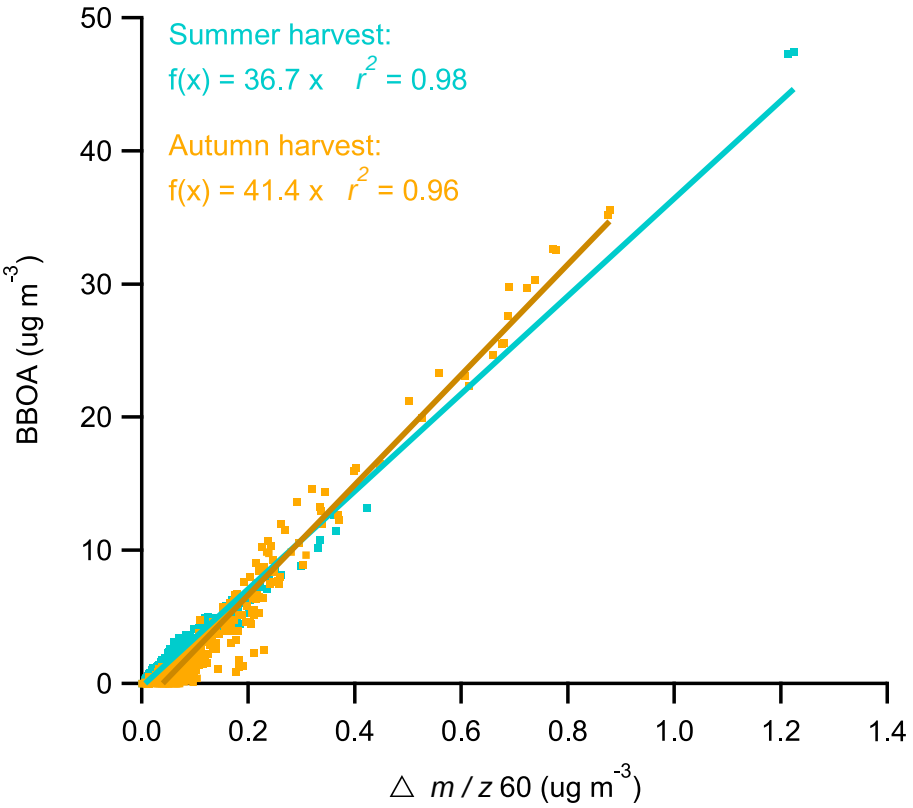

Fig. 9. Correlation plot of BBOA vs. $\Delta m/z$ 60 ($\Delta m/z$ 60 = m/z 60–0.26 % × OA). Note that red dots present the levels of f_{60} in ambient air without BB influence from 1 to 8 July 2013 in this sampling site. The presented background values of f_{60} (around 0.26 ± 0.1 %) are shown in Fig. 8a.

ACPD
14, 9109–9154, 2014

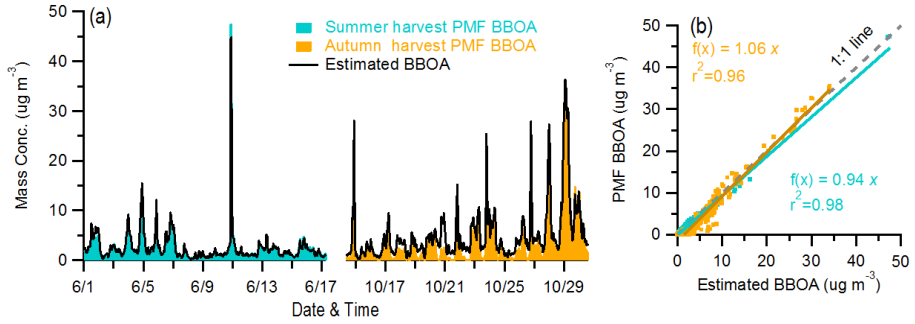

Fig. 10. Time series of BBOA identified by PMF (PMF BBOA) and estimated BBOA during the summer (BBOA = 36.7 × $\Delta m/z$ 60) and autumn (BBOA = 41.4 × $\Delta m/z$ 60) harvest seasons respectively, as well as correlation plot of estimated BBOA vs. PMF BBOA.

ACPD
14, 9109–9154, 2014

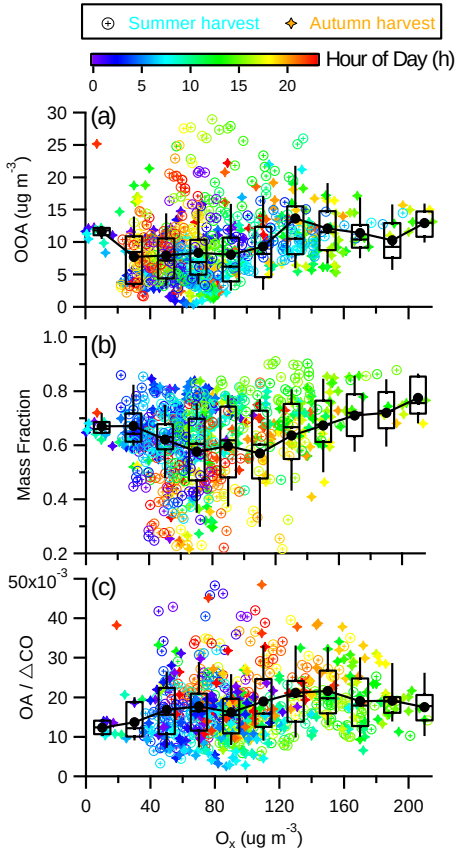

Fig. 11. Variations of **(a)** mass concentration, **(b)** fraction of OA components, and **(c)** ratio of OA to ΔCO, as a function of O_x ($O_x = O_3 + NO_2$) mass loadings.

ACPD
14, 9109–9154, 2014

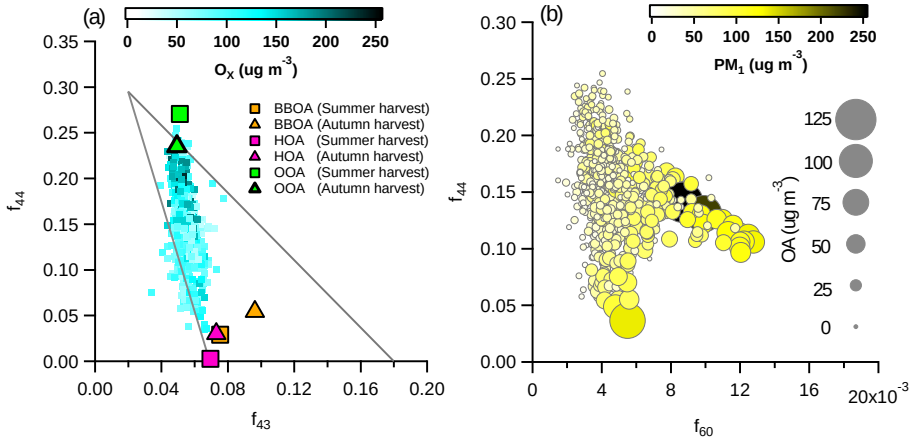

Fig. 12. Summary plots showing **(a)** triangle plot (f_{44} vs. f_{43}); and **(b)** f_{44} as a function of f_{60} (f_{44} vs. f_{60}) for the ambient ACSM datasets during the summer and autumn harvest seasons. The data points are colored by **(a)** the ratio of BBOA/CO; and **(b)** the total PM_1 and mass concentration, as well as sized by the OA mass concentration.

ACPD
14, 9109–9154, 2014

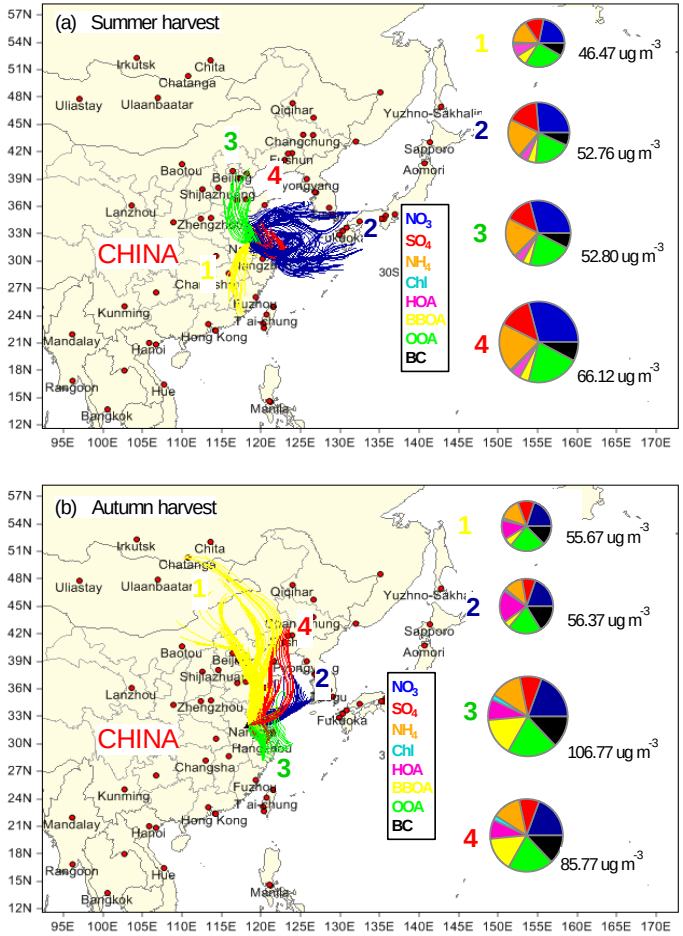

Fig. 13. Calculated 48 h back-trajectories for **(a)** the summer harvest and **(b)** the autumn harvest.

ACPD
14, 9109–9154, 2014

Submicron aerosols during harvest seasons

Y. J. Zhang et al.